Z. Angew. Math. Phys. 61 (2010), 745–772

0044-2275/10/040745-28
published online August 20, 2009
DOI 10.1007/s00033-009-0029-8

Zeitschrift für angewandte Mathematik und Physik ZAMP

Emergence and disappearance of load induced fiber kinking surfaces in transversely isotropic hyperelastic materials

Seungik Baek and Thomas J. Pence

Abstract. The kinematics of shearing deformation in fiber reinforced materials can lead to fibers that (a) first shorten, (b) then return to their original length, and (c) then elongate. In a hyperelastic constitutive treatment this can cause the shear stress to be a nonmonotone function of the amount of shear if the fibers are sufficiently more stiff than the matrix. Here, we explore how this effects the emergence and development of kink surfaces in the context of a variety of boundary value problems. Kink surfaces are surfaces across which the deformation gradient is discontinuous. For fiber reinforced materials such surfaces generate an abrupt change in the fiber orientation (a kink). We characterize the appearance of kink surfaces in terms of three general mechanisms: fade-in, pair creation, and boundary emission. Each has a counterpart for kink surface disappearance. These mechanisms are highly sensitive both to changes in the original fiber orientation field, including spatial variation in this field, and to changes in the nature of the applied boundary conditions. A variety of examples are presented.

Mathematics Subject Classification (2000). 74B20 · 74E05 · 74E10.

Keywords. Hyperelastic · Constitutive behavior · Fiber reinforcement · Kink surfaces · Transverse isotropy.

1. Introduction

Anisotropic hyperelasticity theory provides a natural framework for the modeling of fiber reinforced materials subject to large deformation [22,23,25,26,28]. Such models are of great interest in a variety of fields, a notable example being that of soft tissue mechanical behavior [10]. It is the purpose of this paper to remark on the connection between the so called off-axis shearing response function for fiber reinforced hyperelastic materials, and the presence of internal material surfaces across which the fibers exhibit an abrupt change in orientation. In particular, due to the kinematics of fiber shortening and lengthening in such materials, this off-axis shearing response may be a nonmonotone function of shear. The reason for this phenomena is discussed in detail in [23]. For such materials, the solution to boundary value problems may develop singular surfaces across which there is a jump in the deformation gradient. When such singular surfaces occur in isotropic materials they are sometimes referred to as *elastostatic shocks* [1,2,14]. In the setting of fiber reinforced materials, such jumps introduce a discontinuity in the fiber direction field. For this reason such jumps are often referred to as *kink surfaces* (viz. [8,17,18]).

Boundary value problems that involve such kink surfaces are presented in [12,21]. For these boundary value problems, the standard procedures for the construction of smooth solutions breaks down when some aspect of the boundary conditions exceeds a threshold value. This in turn motivates the consideration of deformation fields containing kink surfaces. The associated loss of smoothness in the deformation field is not unusual if the strain energy function is not convex [9]. Nonconvex energy functions are in turn implicated in the loss of ellipticity in the governing equations. Conditions associated with the loss of ellipticity in hyperelasticity were first investigated in detail in the context of the isotropic theory [13,30]. With the increasing interest in fiber reinforced materials, the ellipticity conditions have been similarly investigated in detail for anisotropic hyperelastic materials [19,20,24]. There are many subtle mathematical connections that can be made between deformations containing singular surfaces and loss of ellipticity

in the governing equations. One of the most interesting and useful of these connections arises from the observation that it is not unusual for a deformation field containing a singular surface to be everywhere elliptic, including therefore adjacent points on opposing sides of a singular surface. However, when this is the case, it is found that the deformation gradients associated with the two adjacent points, when connected by a path of continuous deformation gradients in an appropriate space of deformation gradients, will always contain at least one deformation gradient on the connecting path at which the governing equations cease to be elliptic. Other than these brief introductory remarks for context, it is not our intent here to explore further the connection between kink surfaces and loss of ellipticity, as we instead refer the reader to the papers cited above for more on that matter.

It is instead our purpose here to discuss the relation between the previously mentioned and easily computed off-axis shearing response, and the appearance and disappearance of kink surfaces in problems characterized by a load parameter that is regarded as changing its value in a quasi-static fashion. In particular, we discuss the appearance of kink surfaces as such a load parameter passes through characteristic threshold values. The appearance of a kink surface can then occur by a variety of mechanisms. One type of mechanism results in a kink-surface that involves no initial fiber kinking so that a discontinuous change in the fiber orientation only occurs as the surface continues to develop. We refer to these as kink fade-in processes, and they typically result in the emergence of a single kink surface in the interior of the material. In mathematical parlance, these would be referred to as weak discontinuity surfaces that then develop into strong discontinuity surfaces. In contrast, kink surfaces can instead involve a discontinuity of the fiber orientation at the instant that the kink surface first appears. There are, broadly speaking, two very different ways in which such initially strong discontinuity surfaces can appear. One way is for such a surface to be emitted from a boundary. The other way involves the nucleation of an incipient pair of kink surfaces in the material interior, which then subsequently move apart. Each of the two sibling kink surfaces participating in such pair nucleation will then generally give discontinuous fiber kinking at the instant of nucleation. All of these processes (fade-in, boundary emission, and pair nucleation) have a converse that is associated with kink surface disappearance. In addition, there is the possibility of a more abrupt snap shearing process in which a whole volume of material suddenly changes its fiber orientation field as a quasi-static load parameter passes through a threshold value.

We here discuss how these phenomena relate to each other in the context of a few boundary value problems of relatively increasing complexity. The first such problem that we consider is so simple that many readers might not regard it as a boundary value problem per se. In this endeavor, we focus particular attention not only on the effect of quasi-static change in the boundary conditions, but also on the effect of changing the original orientation of the fibers in the reference configuration. This allows us to provide further direct connection to the off-axis shearing response function. The methods employed here seek to avoid excessive algebraic and computational analysis that would otherwise obscure the connections that we seek to develop. To this end we employ constructive arguments that do not rely on the particular constitutive functions in the hyperelastic model. This permits us to more easily gauge how the off-axis shearing response, which originally arises in the context of homogeneous deformation [23], influences the construction of various inhomogeneous displacement fields. These displacement fields are of particular interest in that they provide solutions to standard boundary value problems, and these solutions involve the emergence and disappearance of fiber kinking surfaces.

2. General constitutive framework

Let $\mathbf{X}$ denote position in the reference configuration, $\mathbf{x}$ denote position in the deformed configuration, and $\mathbf{F} = \partial\mathbf{x}/\partial\mathbf{X}$ denote the deformation gradient tensor. We consider incompressible hyperelastic materials with a single family of reinforcing fibers. The fibers are assumed to be at their natural length in the reference configuration. Incompressibility requires that all deformations obey

$$\det\mathbf{F} = 1. \tag{1}$$

The unit vector $\mathbf{A}$ gives the fiber orientation in the reference configuration. Let $I_4 = \mathbf{FA}\cdot\mathbf{FA} = \mathbf{A}\cdot\mathbf{CA}$ with $\mathbf{C} = \mathbf{F}^{\mathrm{T}}\mathbf{F}$ so that $\sqrt{I_4}$ is the fiber stretch and $\mathbf{a} = \mathbf{FA}/\sqrt{I_4}$ is a unit vector giving the deformed fiber direction in the current configuration. Since $\mathbf{A}$ establishes a preferred direction, it is sometimes convenient to take this direction as one of the coordinate directions. In such a case, let $\mathbf{i}_2$, and $\mathbf{i}_3$ be unit vectors such that $\{\mathbf{A}, \mathbf{i}_2, \mathbf{i}_3\}$ form an orthogonal system.

Following (2.1) of [23] with some small changes in notation, the stored energy density function is taken of the form

$$W(\mathbf{C}) = \frac{1}{2}\mu(I_1 - 3) + \mu\gamma W_{\mathrm{fib}}(I_4), \tag{2}$$

where μ and γ are nonnegative material constants and $I_1 = \mathrm{tr}(\mathbf{C})$. The case $\gamma = 0$ retrieves the standard neo-Hookean model from the isotropic theory. The function $W_{\mathrm{fib}} : (0,\infty) \to [0,\infty)$ is taken to obey $W_{\mathrm{fib}}(1) = 0$, $W'_{\mathrm{fib}}(1) = 0$, $W''_{\mathrm{fib}}(1) = 1$ where the superposed primes denote differentiation. Under these conditions, the various moduli in the infinitesimal theory with transverse isotropy are given in terms of μ and γ as discussed in [23].

The particular form

$$W_{\mathrm{fib}}(I_4) = \frac{1}{2}(I_4 - 1)^2, \tag{3}$$

gives the so-called standard reinforcing model as discussed in detail in [23] and as used in [12,21]. Other hyperelastic modeling possibilities are discussed for example in [11]. The Cauchy stress tensor associated with (2) is (viz. (3.1) of [23])

$$\mathbf{T} = -p\mathbf{I} + \mu\mathbf{F}\mathbf{F}^{\mathrm{T}} + 2\mu\gamma W'_{\mathrm{fib}}(I_4)\mathbf{FA}\otimes\mathbf{FA}, \tag{4}$$

where p is the Lagrange multiplier associated with the constraint (1).

3. Simple shear

In this work, we are concerned with shearing deformations. The homogeneous deformation of simple shear for these type of materials is discussed in detail in [23]. Following that treatment we consider simple shearing within the $(\mathbf{A}, \mathbf{i}_2)$-plane. Thus $\mathbf{i}_3$ is normal to the planes of shear, and the $\mathbf{i}_3$-direction is sometimes referred to as *the axis of shear* [5]. Let $\mathbf{e}_1$ give the *shearing direction* in the $(\mathbf{A}, \mathbf{i}_2)$-plane, and let $\mathbf{e}_2$ be the unit vector obtained by rotating $\mathbf{e}_1$ by $\pi/2$ about the $\mathbf{i}_3$ axis. Define $\mathbf{e}_3 = \mathbf{i}_3$ so that $\{\mathbf{e}_1, \mathbf{e}_2, \mathbf{e}_3\}$ is also a right handed set of unit vectors. If $\mathbf{X} = X_1\mathbf{e}_1 + X_2\mathbf{e}_2 + X_3\mathbf{e}_3$ is the location of a material point in the reference configuration and $\mathbf{x} = x_1\mathbf{e}_1 + x_2\mathbf{e}_2 + x_3\mathbf{e}_3$ gives the material point in the current deformation, then the shearing deformation of interest may be written

$$x_1 = X_1 + \kappa X_2, \quad x_2 = X_2, \quad x_3 = X_3, \tag{5}$$

and κ is said to be the *amount of shear*.

Let $\psi = \arccos(\mathbf{A}\cdot\mathbf{e}_1)$ be the angle that the undeformed fiber makes with the direction of shear. Then

$$\mathbf{e}_1 = \cos\psi\mathbf{A} + \sin\psi\mathbf{i}_2, \quad \mathbf{e}_2 = -\sin\psi\mathbf{A} + \cos\psi\mathbf{i}_2, \tag{6}$$

and $\mathbf{A} = \cos\psi\mathbf{e}_1 - \sin\psi\mathbf{e}_2$. Of special interest is the dependence of the stress on the angle ψ. If $\mathbf{A}$ is parallel to $\mathbf{e}_1$ (i.e., $\psi = 0$) then a simple shearing deformation does not change the fiber length, so that there is no effect of the fibers on the stress response. If $\mathbf{A}$ is perpendicular to $\mathbf{e}_1$ (i.e., $\psi = \pi/2$) then a simple shearing deformation progressively elongates the fibers so that the effect of the fiber reinforcement is to stiffen the stress response above that provided by the neo-Hookean matrix. It is in the remaining case, that in which $\mathbf{A}$ is neither parallel nor perpendicular to $\mathbf{e}_1$, that the most interesting effect arises. In this case, one of the two possible shearing directions always causes the fibers to elongate so that the response is stiffer then that provided by the matrix alone. Shearing in the other direction, however, takes the fibers through three different stages of deformation. These are an initial stage in which the fiber

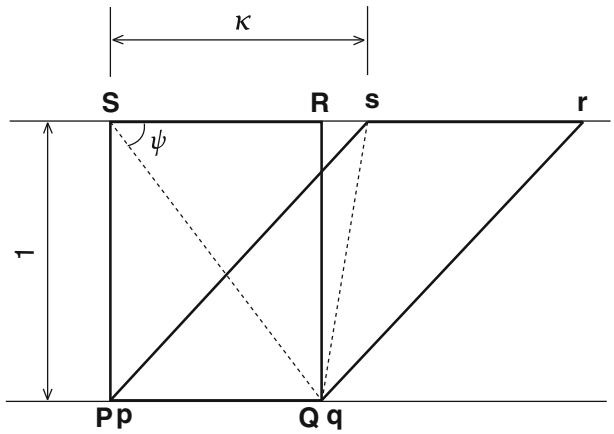

FIG. 1. Illustration of an off-axis shearing deformation. The original rectangle $PQRS$ is deformed into a parallelogram $pqrs$ under simple shear by an amount of κ. The SQ and sq diagonals give the fiber orientation in the reference and deformed configurations respectively

shortens, a second stage in which the fiber returns back to its original length, and a third stage in which the fiber subsequently elongates. The second stage can be regarded as a fiber relaxation stage. It is then the case that the fiber stores strain energy during the first stage that is subsequently released during the second stage. This second stage energy release has the potential to cause the shear stress to be a nonmonotonic function of the amount of shear. This aspect of the homogeneous deformation process is studied in [23]. The consequences of any such nonmonotonic behavior for the solution of boundary values is evident in [12,21].

The deformation gradient associated with the deformation (5) is

$$\mathbf{F} = \mathbf{I} + \kappa \mathbf{e}_1 \otimes \mathbf{e}_2 = \mathbf{I} - \kappa \cos\psi \sin\psi \mathbf{A} \otimes \mathbf{A} + \kappa \cos^2\psi \mathbf{A} \otimes \mathbf{i}_2 \\ -\kappa \sin^2\psi \mathbf{i}_2 \otimes \mathbf{A} + \kappa \sin\psi \cos\psi \mathbf{i}_2 \otimes \mathbf{i}_2. \tag{7}$$

Thus,

$$\mathbf{FA} = (\cos\psi - \kappa \sin\psi)\mathbf{e}_1 - \sin\psi \mathbf{e}_2, \quad I_4 = 1 - 2\kappa \sin\psi \cos\psi + \kappa^2 \sin^2\psi. \tag{8}$$

The aforementioned three stage process as regards the fiber kinematics is now described as follows for the case $0 < \psi < \pi/2$ as illustrated in Fig. 1. This figure shows the rectangle $PQRS$ aligned with the $\mathbf{e}_1$ and $\mathbf{e}_2$ axis in the reference configuration such that the vertical sides $|PS| = |QR| = 1$ and the horizontal sides $|PQ| = |RS| = \cot\psi$. These distances are chosen so that the fiber direction spans the diagonal QS. Note that $|QS| = \sqrt{\cot^2\psi + 1}$. The shearing deformation (5) keeps the base PQ fixed, and deforms the rectangle into a parallelogram $pqrs$ by shifting the top to the right by an amount κ. The initial stage, that of fiber shortening, occurs for $0 < \kappa < k_{(a)} \equiv \cot\psi$. When $\kappa = k_{(a)}$ the fiber that was originally on the diagonal QS has rotated so as to be vertical whereupon its deformed length is reduced to $|qs| = 1$. The second stage, that of fiber relaxation, occurs for $k_{(a)} < \kappa < k_{(b)} \equiv 2\cot\psi$. At $\kappa = k_{(b)}$ the length $|qs|$ is again equal to the length of the reference diagonal $|QS| = \sqrt{\cot^2\psi + 1}$. The third and final stage, that of fiber elongation, occurs for $\kappa > k_{(b)}$.

Turning now to the stress tensor (4) we note that $\mathbf{e}_3$ is an eigenvector of both $\mathbf{FF}^{\mathrm{T}}$ and $\mathbf{FA} \otimes \mathbf{FA}$, so that $\mathbf{e}_3$ gives a principle direction of the Cauchy stress $\mathbf{T}$. Hence we may write

$$\mathbf{T} = T_{11}\mathbf{e}_1 \otimes \mathbf{e}_1 + T_{22}\mathbf{e}_2 \otimes \mathbf{e}_2 + T_{12}(\mathbf{e}_1 \otimes \mathbf{e}_2 + \mathbf{e}_2 \otimes \mathbf{e}_1) + T_{33}\mathbf{e}_3 \otimes \mathbf{e}_3. \tag{9}$$

Expressions for all of these stress components are obtainable from (4). The shear stress T_{12} is independent of the pressure p and corresponds to the shear traction on the horizontal surfaces of the parallelogram

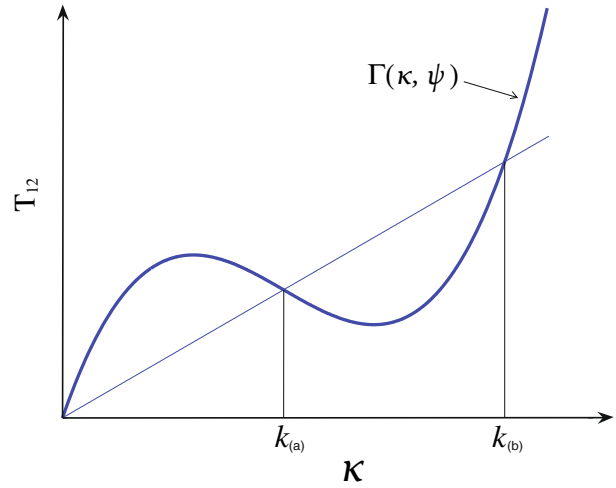

FIG. 2. The off-axis shear response $\Gamma(\kappa,\psi)$ is plotted with respect to κ for a case in which this response is not monotonic. The first stage (fiber shortening) is $0<\kappa\leq k_{(a)}$, the second stage (fiber relaxation) is $k_{(a)}<\kappa<k_{(b)}$, and the third stage (fiber elongation) is $\kappa\geq k_{(b)}$. The linear response represents the off-axis shearing response when $\gamma=0$

pqrs depicted in Fig. 1. One finds that (viz. (4.11) of [23])

$$T_{12}=\mu\kappa-2\mu\gamma\sin\psi(\cos\psi-\kappa\sin\psi)W'_{\rm fib}(1-2\kappa\sin\psi\cos\psi+\kappa^2\sin^2\psi)\equiv\Gamma(\kappa,\psi). \tag{10}$$

The graph of $\Gamma(\kappa,\psi)$ is above the baseline neo-Hookean response during the first and third stages, whereas it is below the baseline neo-Hookean response during the second stage. This is shown in Fig. 2. The baseline neo-Hookean response is a straight line with slope μ and the departure from this baseline response may cause T_{12} to lose monotonicity. Regardless of whether T_{12} is monotone or nonmonotone, the total area above the baseline response during the first stage is the same as the total area below the baseline response during the second stage. This is as one would expect, since these areas correspond to that part of the energy storage and release due solely to the fiber deformation, whereupon the area equality is a consequence of the fiber having returned to its undeformed length when $\kappa=k_{(b)}$.

The function in (10) is central to the connections that we make in this paper. We shall henceforth refer to it as the *shearing response* and, as indicated in (10), shall denote it through the use of the symbol $\Gamma=\Gamma(\kappa,\psi)$. If we wish to emphasize the role of fibers that are neither parallel to the shearing direction ($\psi=0$) nor perpendicular to the shearing direction ($\psi=\pi/2$) then we may refer to this as the *off-axis shearing response*.

In contrast to the off-axis shearing response, the expressions for the normal stress components T_{11}, T_{22}, and T_{33} all contain p, for example

$$T_{22}=-p+\mu+2\mu\gamma\sin^2\psi W'_{\rm fib}(1-2\kappa\sin\psi\cos\psi+\kappa^2\sin^2\psi). \tag{11}$$

The stored energy $W(\mathbf{C})$ in (2) can be expressed directly as a function of the amount of shear κ for this deformation, i.e.

$$W(\mathbf{C})=\frac{1}{2}\mu\kappa^2+\mu\gamma W_{\rm fib}(1-2\kappa\sin\psi\cos\psi+\kappa^2\sin^2\psi)\equiv\tilde{W}(\kappa,\psi). \tag{12}$$

Notice that (10) gives

$$\Gamma(\kappa,\psi)=\frac{\partial}{\partial\kappa}\tilde{W}(\kappa,\psi). \tag{13}$$

4. Nonmonotonic off-axis shearing response

For the standard reinforcing (3) it follows that

$$\Gamma(\kappa,\psi)=\mu\kappa+2\mu\gamma\kappa\sin^2\psi(\cos\psi-\kappa\sin\psi)(2\cos\psi-\kappa\sin\psi). \tag{14}$$

Nonmonotonicity occurs for (14) if $\gamma>2/\sin^2 2\psi$. This is equivalent to $\gamma>2$ and either

$$\frac{1}{2}\arcsin\left(\sqrt{2/\gamma}\right)\leq\psi\leq\frac{\pi}{2}-\frac{1}{2}\arcsin\left(\sqrt{2/\gamma}\right), \tag{15}$$

or

$$-\frac{\pi}{2}+\frac{1}{2}\arcsin\left(\sqrt{2/\gamma}\right)\leq\psi\leq-\frac{1}{2}\arcsin\left(\sqrt{2/\gamma}\right). \tag{16}$$

If $\gamma>2$ then the nonmonotone response occurs for positive κ if (15) holds, whereas the nonmonotone response occurs for negative κ if (16) holds. Consider $\gamma>2$ with (15). Then Γ decreases in κ on the interval $k_{\max}<\kappa<k_{\min}$ where

$$k_{\max}=k_{\max}(\psi,\gamma)=\frac{1}{\tan\psi}-\frac{\sqrt{12\gamma^2\cos^2\psi\sin^2\psi-6\gamma}}{6\gamma\sin^2\psi} \tag{17}$$

and

$$k_{\min}=k_{\min}(\psi,\gamma)=\frac{1}{\tan\psi}+\frac{\sqrt{12\gamma^2\cos^2\psi\sin^2\psi-6\gamma}}{6\gamma\sin^2\psi} \tag{18}$$

locate the respective local maximum and local minimum of the stress response $\Gamma(\kappa,\psi)$ as a function of κ. Furthermore, if $\gamma>8/\sin^2 2\psi$ then this nonmonotonic response causes T_{12} to dip below the κ-axis since one finds that $\gamma>8/\sin^2 2\psi$ gives $\Gamma(k_{\min}(\psi,\gamma),\psi)<0$. The various possibilities discussed above are depicted in Fig. 3.

While the formulae (14)–(18) are specific to the standard reinforcing model, nonmonotonicity of Γ occurs for other $W_{\rm fib}(I_4)$ if γ is sufficiently large. We shall then continue to use the symbols $k_{\max}$ and $k_{\min}$ to indicate the locations of the local extrema, although they will in general no longer be given by the particular expressions (17) and (18). When Γ has this type of nonmonotonic response such that two increasing branches are separated by a decreasing branch, we shall refer to the ascending branch containing $\kappa=0$ as the *primary branch* while the other ascending branch shall be dubbed the *secondary branch*. The intermediate branch between the primary and secondary branch will be referred to either as the descending branch or as the unstable branch. It is important to realize that these different branches do not correlate directly with the three stage fiber kinematics discussed in the previous section if, for no other reason, then that the three stage fiber kinematics always takes place in simple shear, whereas nonmonotonicity may or may not occur. Furthermore, when nonmonotonicity does occur, say for $\kappa>0$, it will then be the case that $0<k_{\max}<k_{(a)}<k_{\min}<k_{(b)}$.

If $\Gamma(\kappa,\psi)$ is monotone then it has a unique inverse function, say $\Lambda(T,\psi)$. This means that $\Lambda(\Gamma(\kappa,\psi),\psi)=\kappa$ and $\Gamma(\Lambda(T,\psi),\psi)=T$. If, however, $\Gamma(\kappa,\psi)$ is nonmonotone then there does not exist a unique inverse, since values T obeying $\Gamma(k_{\min},\psi)<T<\Gamma(k_{\max},\psi)$ have three associated values of κ that give $\Gamma(\kappa,\psi)=T$. This has important consequences for both homogeneous deformation, which can be investigated directly, and for nonhomogeneous deformations that arise from the solution of boundary value problems.

Consider an infinite layer $-\infty<X_1<\infty$, $0<X_2<H$, $-\infty<X_3<\infty$ of such a fiber reinforced material where ψ is a constant and the layer is subject to fixed displacement conditions on the lower surface $X_2=0$. On the upper surface take conditions of zero normal traction and specified shear traction. We write this boundary condition as

$$\mathbf{t}=T_{\rm app}\mathbf{e}_1\quad\text{on}\quad X_2=H. \tag{19}$$

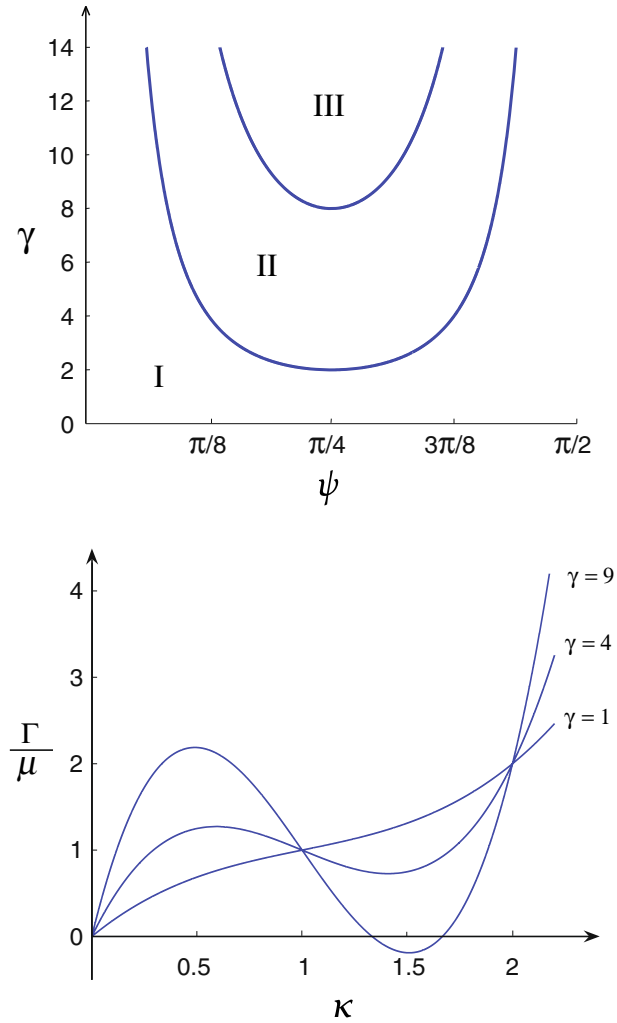

FIG. 3. The correlation of the three different types of shear response with γ and ψ for the standard reinforcing model. *Above* when $(\gamma,\ \psi)$ is within region I the shear response is monotonic. In region II the response is nonmonotonic and positive for all $\kappa > 0$. In region III the response is nonmonotonic and there exists an interval of $\kappa > 0$ where $\Gamma(\kappa, \psi)$ becomes negative. *Below* examples of these different shear responses for $\gamma = 1$, $\psi = \pi/4$ (region I), $\gamma = 4$, $\psi = \pi/4$ (region II), and $\gamma = 9,\ \psi = \pi/4$ (region III)

When $\Gamma(\kappa, \psi)$ is monotone then the unique inverse $\Lambda(T_{\rm app}, \psi)$ gives the value of κ associated with a unique simple shearing deformation (5) consistent with (19). This traction condition requires that $T_{22} = 0$ which, in view of (11), is met by taking

$$p = \mu + 2\mu\gamma \sin^2\psi W'_{\rm fib}(1 - 2\kappa \sin\psi\cos\psi + \kappa^2 \sin^2\psi) \equiv \tilde{p}_o(\kappa, \psi) \tag{20}$$

with $\kappa = \Lambda(T_{\rm app}, \psi)$.

Suppose now, for this same rather trivial boundary value problem, that Γ is nonmonotone. Then values of $T_{\rm app}$ obeying $\Gamma(k_{\rm min}, \psi) < T_{\rm app} < \Gamma(k_{\rm max}, \psi)$ have three separate simple shearing deformation solutions corresponding to the three values κ that give $\Gamma(\kappa, \psi) = T_{\rm app}$. In addition, it is also possible to consider *alternating layer solutions*. An alternating layer solution is a stack of (sub)layers, each with a constant shearing using one of the three different fixed values of κ determined by $T_{\rm app}$. For such

alternating layer solutions, the separating planes have normal $\mathbf{e}_2$ and hence traction continuity requires continuity of T_{12}, T_{22} and T_{32} across these separating planes. Since T_{32} vanishes identically, the last of these three conditions is automatic. Continuity of T_{12} is also automatically satisfied since Γ has the same value for each of the three possible values of κ. Continuity of T_{22} is achieved by again taking $p = \tilde{p}_o(\kappa, \psi)$ using the local value of κ. Hence both κ and p are discontinuous across any such separating plane. The deformation itself is described by the formulae (5) in the layer that is on the bottom (using the appropriate value of κ for that layer). However, any layers above the lowest layer will require the simple modification $x_1 = X_1 + \kappa X_2 + \text{constant}$, where the constant is chosen so as to keep x_1 continuous. While the deformation is continuous, the discontinuous change in κ generates an abrupt change in the deformed fiber direction field across each such surface, motivating the terminology *kink surface*.

Problems of this kind for isotropic materials, namely problems in which multiple solutions naturally arise due to a nonmonotonic stress response, received a great deal of attention in the 1970s and 1980s beginning with the influential paper of Ericksen [7]. In the present discussion, let us for the moment return attention to homogeneous deformation simple shearing solutions (5) as T_{app} is slowly increased from $T_{\text{app}} = 0$. Thus we are now considering a quasi-static problem where increasing T_{app} plays the role of time. In this setting, one possible way of constructing these simple shearing solutions is to take solutions associated with the primary branch for as long as this is possible. This is the so called *maximum delay* convention, and results in a continuously increasing κ so long as $T_{\text{app}} < \Gamma(k_{\max}, \psi)$. Under this convention, solutions then transition to the secondary branch at $T_{\text{app}} = \Gamma(k_{\max}, \psi)$. At the time of this transition there is an abrupt change in κ and hence a snapping through from one configuration to another configuration. Further increase in T_{app} then results once again in a continuously increasing κ as the loading is now confined to the secondary branch. Unloading gives rise to a similar issue in that a decrease in T_{app} requires a jump back to the primary branch if T_{app} decreases below the value $\Gamma(k_{\min}, \psi)$. The maximum delay convention then involves taking this backward jump at $T_{\text{app}} = \Gamma(k_{\min}, \psi)$.

More generally for such homogeneous deformation solutions, let $T_\uparrow$ be the value of T_{app} at which there is a jump from the primary branch to the secondary branch for increasing T_{app}. Similarly, let $T_\downarrow$ be the value of T_{app} at which there is a jump from the secondary branch to the primary branch for decreasing T_{app}. Elementary stability arguments provide justification for dismissing solutions that involve values of κ on the middle branch of Γ in which the graph is decreasing. A particularly simple type of model takes $T_\uparrow$ and $T_\downarrow$ as specified. For example, they could be regarded either as a fixed material property or as a material property that depends on prevailing conditions such as for example the temperature. Prevailing conditions might also include a concept of system noise such that low noise favors the maximum delay convention whereas high noise promotes an earlier transition. Elementary energy arguments, based for example on hysteresis loops in cyclic processes [15], then give that $T_\uparrow \geq T_\downarrow$.

The analysis of Ericksen [7] followed by that of Abeyaratne and Knowles among others (see, e.g., [2–4,6,14,27]) can be applied to the problem under consideration here. This provides further insight into the possibilities for $T_\uparrow$ and $T_\downarrow$. The energy argument that is given in the remainder of this section is a standard one that is based on such considerations, and the reader is referred to [4] and [7] for additional clarification. For the moment, we continue to restrict attention to a homogeneous simple shearing deformation (5) that is associated with the load parameter T_{app} as this parameter changes with time in a quasi-static manner. Consider the following energy argument as applied to a square prism in the reference configuration whose base is a unit square in the (X_1, X_3)-plane. The work of the external surface tractions on this prism between generic times $t_{(1)}$ and $t_{(2)}$ is

$$\text{Work} = \int_{\kappa|_{t_{(1)}}}^{\kappa|_{t_{(2)}}} \Gamma(\kappa, \psi) H \, \mathrm{d}\kappa, \tag{21}$$

whereas the change in elastic energy stored within the prism between these same two times is

$$\text{Storage} = \{\tilde{W}(\kappa|_{t_{(2)}}, \psi) - \tilde{W}(\kappa|_{t_{(1)}}, \psi)\}H. \tag{22}$$

For processes in which κ remains confined to the same branch of the shearing response Γ it follows that the energy storage (22) is equal to the work (21) by virtue of (13). However, a jump between branches generally causes the work to be unequal to the storage. In this case, a standard view of the second law of thermodynamics is that the change in energy storage cannot exceed the work (see again [4]).

Suppose that such a jump between branches occurs at $t = t_*$ such that the layer is deformed according to (5) both just before and just after $t = t_*$. Denote the homogeneous shearing value just before the time of the jump by κ_*^-. Denote the homogeneous shearing value just after the time of the jump by κ_*^+. Let T_* be the value of the applied shearing traction T_{app} at the time of the jump so that $T_* = \Gamma(\kappa_*^-, \psi) = \Gamma(\kappa_*^+, \psi)$. The second law restriction may then be written directly as

$$\{\tilde{W}(\kappa_*^+, \psi) - \tilde{W}(\kappa_*^-, \psi)\}H \leq (\kappa_*^+ - \kappa_*^-)HT_* \tag{23}$$

where it is to be emphasized that κ_*^+ and κ_*^- give values of shearing at different times (not different locations) and that there is as yet no assumption as to which of the two values is greater. Nor is there yet any assumption as to which value belongs to the primary branch and which belongs to the secondary branch.

The case of equality in (23) is of special significance. In this case, (23) can be written as

$$\tilde{E}(\kappa_*^-, \psi) = \tilde{E}(\kappa_*^+, \psi), \qquad \Gamma(\kappa_*^-, \psi) = \Gamma(\kappa_*^+, \psi), \tag{24}$$

where

$$\tilde{E}(\kappa, \psi) \equiv \tilde{W}(\kappa, \psi) - \kappa \frac{\partial}{\partial \kappa} \tilde{W}(\kappa, \psi). \tag{25}$$

These have a well-known geometrical interpretation with respect to the graph of Γ. Namely, $\Gamma(\kappa_*^-, \psi) = \Gamma(\kappa_*^+, \psi)$ is the value of stress with the property that a horizontal line at this stress intersects the graph of Γ at three points in such a fashion so as to create two regions that are of equal area. The special value of stress with this property is known as the *Maxwell stress* and will be denoted here by T_{jcm}. Furthermore, let the value of κ on the primary branch associated with the above equal area construction be denoted by $k_{\text{jcm}\uparrow}$, let the value of κ on the secondary branch associated with this construction be denoted by $k_{\text{jcm}\downarrow}$, and let the excluded value of κ on the unstable branch that is associated with this construction be denoted by $k_{\text{jcm}\leftrightarrow}$.

To describe a jump from the primary branch to the secondary branch during the homogeneous shearing, take κ_*^- on the primary branch, κ_*^+ on the secondary branch, and $T_* = T_\uparrow$. Then (23) yields $T_\uparrow \geq T_{\text{jcm}}$. In a similar fashion (23) applied to a jump from the secondary branch to the primary branch gives $T_\downarrow \leq T_{\text{jcm}}$. Together these give

$$T_\uparrow \geq T_{\text{jcm}} \geq T_\downarrow. \tag{26}$$

In particular, the Maxwell value is the only value of stress for which jumps are permitted in either direction. Treatments based on restricting jumps to the Maxwell value naturally deliver energy minimal configurations [2,7]. Conversely, hysteretic treatments are associated with dissipative phenomena since then (23) is a strict inequality.

Although the argument leading to (26) is reviewed above in the context of homogeneous deformation quasi-static processes, such arguments also apply to the treatment of the alternating layer solutions. This is done by localizing the argument to a neighborhood of each discontinuity surface and again gives that energy minimal configurations require that $T_{12} = T_{\text{jcm}}$ on both sides of any such jump. Furthermore, energy minimal configurations of the overall problem, i.e., the problem characterized by a specified boundary value T_{app} in (19), can only involve a kink surface if $T_{\text{app}} = T_{\text{jcm}}$. Thus the minimum energy problem does not admit layer solutions if $T_{\text{app}} \neq T_{\text{jcm}}$. Hence there is a unique energy minimal solution given by the primary branch homogeneous deformation (5) when $T_{\text{app}} < T_{\text{jcm}}$ and there is also a unique energy

minimal solution given by the secondary branch homogeneous deformation (5) when $T_{\rm app} > T_{\rm jcm}$. Alternating layer solutions are energy minimal solutions only for $T_{\rm app} = T_{\rm jcm}$ and such solutions involve any sequence of alternating layers across which the shearing strain jumps between $k_{\rm jcm\uparrow}$ and $k_{\rm jcm\downarrow}$. For $T_{\rm app} = T_{\rm jcm}$ the arbitrary nature of these energy minimizing alternating layer sequences then allows the top surface to displace in the $\mathbf{e}_1$ direction by any amount in the interval $k_{\rm jcm\uparrow} H \leq (x_1 - X_1)|_{X_2=H} \leq k_{\rm jcm\downarrow} H$.

For the standard reinforcing model (3) one finds that $k_{\rm jcm\leftrightarrow} = k_{(a)} = \cot\psi$. In words, the unstable value of Maxwell shearing $k_{\rm jcm\leftrightarrow}$ in the standard reinforcing model corresponds to the the unique value of shear associated with maximal fiber contraction $k_{(a)}$. One then also verifies for the standard reinforcing model that

$$k_{\rm jcm\uparrow} = \cot\psi - \frac{\sqrt{2\gamma\sin^2\psi\cos^2\psi - 1}}{\sqrt{2\gamma}\sin^2\psi}, \tag{27}$$

$$k_{\rm jcm\downarrow} = \cot\psi + \frac{\sqrt{2\gamma\sin^2\psi\cos^2\psi - 1}}{\sqrt{2\gamma}\sin^2\psi}. \tag{28}$$

The Maxwell stress is then given by $T_{\rm jcm} = \Gamma(k_{\rm jcm\uparrow}, \psi) = \Gamma(k_{\rm jcm\leftrightarrow}, \psi) = \Gamma(k_{\rm jcm\downarrow}, \psi) = \mu\cot\psi$, and one also finds that $\tilde{E}(k_{\rm jcm\uparrow}, \psi) = \tilde{E}(k_{\rm jcm\downarrow}, \psi) = -\mu/(8\gamma\sin^4\psi)$. All of the results in this section can be regarded as well known on the basis of, for example, [7,2,23].

When Γ is a nonmonotone function of κ let $\Lambda_{\rm jcm}(T, \psi)$ be the particular inverse associated with jumping between the two ascending branches of Γ at the Maxwell value $T_{\rm jcm}$. For the standard reinforcing model, since (14) is cubic in κ, one may write a formal expression for $\Lambda_{\rm jcm}(T, \psi)$ on the separate domains $T < T_{\rm jcm}$ and $T > T_{\rm jcm}$. The resulting expressions are cumbersome in nature and so will not be displayed here (see, e.g., Eqs. (44), (45), (52), and (54) of [12]). More generally, if Γ is a nonmonotone function of κ and we wish to consider hysteretic processes such that $T_\uparrow > T_\downarrow$ then it may be convenient to define directionally dependent inverse functions $\Lambda_\uparrow(T, \psi, T_\uparrow)$ and $\Lambda_\downarrow(T, \psi, T_\downarrow)$. Note in this case that if either $T_\uparrow$ or $T_\downarrow$ approaches the Maxwell value $T_{\rm jcm}$, then the corresponding inverse function approaches the Maxwell inverse $\Lambda_{\rm jcm}(T, \psi)$.

5. Maxwell solutions for an undulatory fiber orientation field subject to shear traction

In this section, we restrict attention to energy minimizing solutions for the previously considered layer subject to the same boundary conditions of holding $X_2 = 0$ fixed and specifying zero normal traction and nonzero shear traction (19) on the top surface. However, we now allow for the possibility that the undeformed fiber direction angle can vary with the X_2 location in the layer. The discussion of the previous section established that if ψ is a constant, say ψ_o, such that $\Gamma(\kappa, \psi_o)$ is not monotonic, then energy minimizing solutions evolve as follows as $T_{\rm app}$ is increased. For $T_{\rm app} < T_{\rm jcm}$ there is a unique solution given by the homogeneous deformation (5) and the shear κ for this solution is on the primary branch of the shearing response $\Gamma(\kappa, \psi_o)$. In particular, the displacement of the top surface is continuously increasing with $T_{\rm app}$. Then, as $T_{\rm app}$ passes through the value $T_{\rm jcm}$, the layer experiences an abrupt jump in shear such that the top surface displaces by the amount $(k_{\rm jcm\downarrow} - k_{\rm jcm\uparrow})H$. After this jump the displacement is once again a continuously increasing function of the applied load $T_{\rm app}$ since the shear now increases on the secondary branch. Unloading $T_{\rm app}$ reverses the process, and in particular the layer snaps back to the primary branch as the load decreases through $T_{\rm jcm}$.

We now consider the effect of a spatially varying fiber orientation field by taking $\psi = \hat{\psi}(X_2)$ in the context of the same boundary value problem of a layer with thickness H. For energy minimizing solutions it can again be shown that kink surfaces must satisfy the Maxwell stress condition that $T_{12} = T_{\rm jcm}$ on each side of the kink surface. The variable fiber direction field is taken to be the only source of inhomogeneity.

In particular, μ and γ do not change with location. The off-axis shearing response $\Gamma(\kappa, \hat{\psi}(X_2))$ is now a function of X_2, and so whether or not this function is monotonic in κ will generally depend on the value of X_2. For those X_2 at which $\Gamma(\kappa, \hat{\psi}(X_2))$ is nonmonotone we shall let $\hat{T}_{\rm jcm}(X_2)$ be the local value of the Maxwell stress. Under these circumstances, the Maxwell strains $k_{\rm jcm\uparrow}$ and $k_{\rm jcm\downarrow}$ also become functions of position, say $\hat{k}_{\rm jcm\uparrow}(X_2)$ and $\hat{k}_{\rm jcm\downarrow}(X_2)$. For the standard reinforcing (3) the functions $\hat{k}_{\rm jcm\uparrow}(X_2)$ and $\hat{k}_{\rm jcm\downarrow}(X_2)$ are obtained by entering (27) and (28) with $\psi = \hat{\psi}(X_2)$, while $\hat{T}_{\rm jcm}(X_2) = \mu \cot \hat{\psi}(X_2)$. More generally,

$$\hat{T}_{\rm jcm}(X_2) = \Gamma(\hat{k}_{\rm jcm\uparrow}(X_2), \hat{\psi}(X_2)) = \Gamma(\hat{k}_{\rm jcm\downarrow}(X_2), \hat{\psi}(X_2)). \tag{29}$$

If $\Gamma(\kappa, \hat{\psi}(X_2))$ is a true function of X_2 then it is no longer possible to construct equilibrium solutions of the type considered in the previous section in which the deformation gradient $\mathbf{F}$ is of the form (7) either throughout the whole layer or in individual sublayers. Motivated by the need to generalize (5), consider deformations of the form

$$x_1 = X_1 + f(X_2), \quad x_2 = X_2, \quad x_3 = X_3. \tag{30}$$

The function $f(X_2)$ is called the *rectilinear shear* and deformations of this form are considered in [16,29]. The deformation gradient is given by (7) under the replacement

$$\kappa \to \frac{\partial f}{\partial X_2} \equiv f'(X_2). \tag{31}$$

It then follows that $T_{12} = \Gamma(f'(X_2), \hat{\psi}(X_2))$. Thus T_{12} is equal to $T_{\rm app}$ everywhere in the layer provided that

$$\Gamma(f'(X_2), \hat{\psi}(X_2)) = T_{\rm app}. \tag{32}$$

Taking (32) as an equation for the determination of $f'(X_2)$ one may then take $p = \tilde{p}_o(f'(X_2), \hat{\psi}(X_2))$ with $\tilde{p}_o$ again given by (20) whereupon it follows that T_{22} once again vanishes identically. It then follows that the Cauchy stress $\mathbf{T}$ is of the form

$$\mathbf{T} = T_{11}(X_2)\mathbf{e}_1 \otimes \mathbf{e}_1 + T_{\rm app}(\mathbf{e}_1 \otimes \mathbf{e}_2 + \mathbf{e}_2 \otimes \mathbf{e}_1) + T_{33}(X_2)\mathbf{e}_3 \otimes \mathbf{e}_3. \tag{33}$$

Thus both the equation of equilibrium $\mathrm{div}\mathbf{T} = \mathbf{0}$ and the traction boundary condition (19) are satisfied identically. Kink surfaces are also naturally constructed by this development since (33) gives that the traction on each side of a kink surface is $\mathbf{t} = T_{\rm app}\mathbf{e}_1$ and hence is continuous. The function $f(X_2)$ follows by integration using $f(0) = 0$ and continuity of f across any kink surface. Since we are in this section restricting attention to energy minimizing configurations, a necessary condition for the deformation field to contain a kink surface is that $T_{\rm app}$ coincides with $\hat{T}_{\rm jcm}(X_2)$ for some X_2 locations in the layer.

We shall illustrate how this works by again considering the the standard reinforcing (3). Let $0 < \psi_o < \pi/2$ and $\gamma > 0$ be such that $\gamma > 2/\sin^2 2\psi_o$. Then for the case of a constant fiber direction field with $\psi = \psi_o$ there will be an abrupt shearing at $T_{\rm app} = \mu \cot \psi_o$. Now suppose that the fiber direction field fluctuates about such a constant direction, in particular take periodic fluctuations (undulations) such that

$$\psi = \hat{\psi}(X_2) = \psi_o + \delta_o \sin(\omega X_2) \tag{34}$$

for some positive δ_o and ω. The undulation length is $2\pi/\omega$ and many undulations will occur across the layer width provided that $\omega >> 2\pi/H$.

As a first undulatory example take $\pi/4 < \psi_o < \pi/2$ and δ_o sufficiently small so that $\psi_o - \delta_o > \pi/4$ and $\psi_o + \delta_o < \pi/2$. Assume also that $\gamma > 2/\sin^2 2(\psi_o + \delta_o)$. Under these restrictions the undulations give a relatively small orientation angle perturbation and $\Gamma(\kappa, \hat{\psi}(X_2))$ remains nonmonotonic for all X_2. Now increasing $T_{\rm app}$ from zero first causes the Maxwell condition to be met when $T_{\rm app} = \mu \cot(\psi_o + \delta_o)$. This occurs at a finite number of locations given by $X_2 = \pi/2\omega + 2n\pi/\omega$ with $n = 0, 1, \ldots, N$ where N is the greatest integer such that $1/2 + 2N \leq H\omega/\pi$. As $T_{\rm app}$ increases through $\mu \cot(\psi_o + \delta_o)$ each of

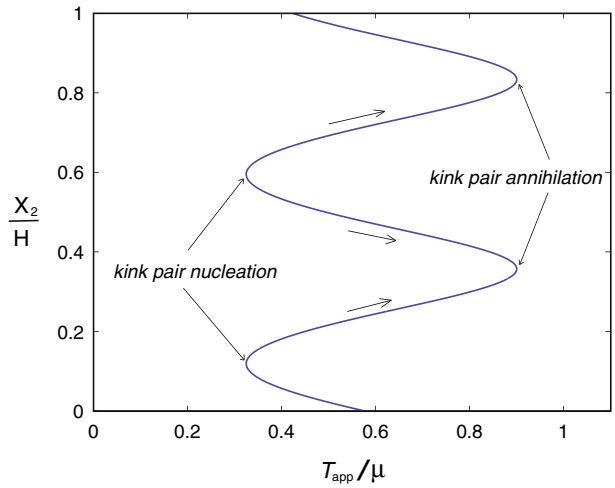

FIG. 4. Applied shear traction versus the location of fiber kinking surfaces as determined by the Maxwell condition. The depiction is for Case 1, i.e., $\gamma > 2\ Max[1/\sin^2 2(\psi_o + \delta_o), 1/\sin^2 2(\psi_o - \delta_o)]$, and the fiber direction field varies with X_2 according to (34). When $T_{\rm app}$ is increased from zero, kink pairs are first nucleated when $T_{\rm app}/\mu = \cot(\psi_o + \delta_o)$. The two sibling kinks separate by moving in opposite directions as $T_{\rm app}$ increases. Non-sibling kinks then encounter each other and disappear (kink pair annihilation) when $T_{\rm app}/\mu = \cot(\psi_o - \delta_o)$. In the figure, parameters for (34) are given by $\psi_o = \pi/3$, $\delta_o = \pi/15$, and $\omega = 4.2\pi/H$. This example also shows kink emission at $X_2 = H$ and kink absorption at $X_2 = 0$ for special values of $T_{\rm app}$

these locations gives rise to two kink surfaces in a process that can be referred to as *kink pair nucleation*. The two kink surfaces then separate as $T_{\rm app}$ increases. In particular, one of these sibling kink surfaces increases its X_2 value with further increase in $T_{\rm app}$ while the other sibling kink surface decreases its X_2 value. Between these two kink surfaces the value of f' is associated with the secondary branch of the local shear response function $\Gamma(\kappa, \hat{\psi}(X_2))$. While each such kink surface is moving away from its sibling on one side, it is at the same time approaching a different kink surface on its other side. All of the approaching kink surfaces meet and mutually annihilate when $T_{\rm app}$ reaches the value $\mu\cot(\psi_o - \delta_o)$ in a process of *kink pair annihilation*. For $T_{\rm app} > \mu\cot(\psi_o - \delta_o)$ all values of f' are now associated with the local secondary branch of the off-axis shearing response curve. By virtue of this kink surface motion, there is no longer an abrupt snap-through displacement at $T_{\rm app} = \mu\cot\psi_o$ but rather a continuous increase in displacement over the load interval $\mu\cot(\psi_o + \delta_o) < T_{\rm app} < \mu\cot(\psi_o - \delta_o)$. It is to be remarked that the above text description of kink surface motion requires modification near the external boundaries $X_2 = 0$ and $X_2 = H$. This is because kink surfaces may also emerge from an external surfaces (kink emission at an external boundary) and disappear into an external surface (kink absorption at an external boundary).

Figure 4 represents the quasi-static motion of the various kink surfaces that we have just described in a diagram where the horizontal axis gives $T_{\rm app}$ and the vertical axis gives $x_2 = X_2$ on the interval $0 \le X_2 \le H$. The phenomena under consideration here arise because the Maxwell stress $T_{\rm jcm}$ is a function of position by virtue of $\psi = \hat{\psi}(X_2)$ as we have already made explicit by means of the function $\hat{T}_{\rm jcm}(X_2)$ in (29). The locus of values $(T_{\rm app}, X_2)$ satisfying $T_{\rm app} = \hat{T}_{\rm jcm}(X_2)$ in Fig. 4 represents the quasi-static motion of the kink surface as $T_{\rm app}$ changes. In particular, locations where this locus is vertical correspond either to kink pair creation or to kink pair annihilation as determined by whether $T_{\rm app}$ is increasing or decreasing. Specifically, if $T_{\rm app}$ is increasing then the vertical locus points that are a local minimum of the function $\hat{T}_{\rm jcm}(X_2)$ correspond to kink pair creation while those that correspond to a local maximum correspond to kink pair annihilation.

In the just concluded example, the inequality condition $\psi_o - \delta_o > \pi/4$ was not essential. The reason for imposing the condition $\psi_o - \delta_o > \pi/4$ was to ensure that $\Gamma(\kappa, \hat{\psi}(X_2))$ was nonmonotone for all X_2.

Thus the restriction $\psi_o - \delta_o > \pi/4$ could have been dropped from the list of requirements in the previous example so long as the inequality condition on γ was instead taken to be $\gamma > \text{Max}[2/\sin^2 2(\psi_o + \delta_o), 2/\sin^2 2(\psi_o - \delta_o)]$. This raises the question as to the consequences of $\Gamma(\kappa, \hat{\psi}(X_2))$ being monotone for some X_2 and nonmonotone for the other X_2. Consider, again the same undulatory direction field (34), such that now $0 < \psi_o < \pi/2$ with $\gamma > 2/\sin^2 2\psi_o$ and $\delta_o > 0$ sufficiently small so that $0 < \psi_o - \delta_o < \psi_o + \delta_o < \pi/2$. These parameters can be chosen in various ways so as to give any of the following four cases:

$$\begin{aligned}
&\textit{Case } 1 \quad && \gamma > 2\text{Max}[\csc^2 2(\psi_o + \delta_o), \csc^2 2(\psi_o - \delta_o)],\\
&\textit{Case } 2 \quad && 2\csc^2 2(\psi_o - \delta_o) > \gamma > 2\csc^2 2(\psi_o + \delta_o),\\
&\textit{Case } 3 \quad && 2\csc^2 2(\psi_o + \delta_o) > \gamma > 2\csc^2 2(\psi_o - \delta_o),\\
&\textit{Case } 4 \quad && \gamma < 2\text{Min}[\csc^2 2(\psi_o + \delta_o), \csc^2 2(\psi_o - \delta_o)].
\end{aligned}$$

Case 1 corresponds to the previously considered example that generates Fig. 4 in which the essential feature is that $\Gamma(\kappa, \hat{\psi}(X_2))$ is nonmonotone for all X_2. As indicated in the previous description, the kink surfaces which appear in the interior of the layer do so by first nucleating an incipient pair of kinks which then separate and move apart. The kink surfaces which disappear in the interior of the layer do so by encountering the particular kink surface toward which it had been moving. These processes of kink pair nucleation and kink pair annihilation involve finite jumps in f' at each kink surface both just after pair nucleation and just before pair annihilation.

In contrast to case 1, the remaining cases 2–4 involve monotone $\Gamma(\kappa, \hat{\psi}(X_2))$ for some X_2. However, since we are still keeping $\gamma > 2\csc^2 2\psi_o$ there will be certain locations (e.g., $X_2 = n\pi/\omega$ for integers n) at which the response is nonmonotone. In discussing cases 2–4 we again consider the quasi-static response as T_{app} increases from zero using the Maxwell criterion at all kink surfaces.

When considering case 2, the response in this case mirrors that described in case 1 for the emergence and early motion of the kink surfaces. Namely kink pairs emerge at $T_{\text{app}} = \mu\cot(\psi_o + \delta_o)$ and these siblings then begin to move apart under increasing T_{app}. However, the nonmonotonicity condition ceases to be met once these kink surfaces reach locations at which $\psi = (1/2)\arcsin\sqrt{2/\gamma}$, a condition which is guaranteed to occur by virtue of the inequality $\gamma < 2\csc^2 2(\psi_o - \delta_o)$. Thus the kink surfaces do not disappear by pair annihilation, rather they progressively weaken as they approach the locations X_2 at which $\psi = (1/2)\arcsin\sqrt{2/\gamma}$. At these locations the $\Gamma(\kappa, \hat{\psi}(X_2))$ response transitions from nonmonotone to monotone and the associated kink surface disappears by simply fading out (henceforth referred to as *kink fade out*). This is represented in Fig. 5.

Before moving on to the consideration of case 3 let us consider unloading of both case 1 and case 2 from a value T_{app} that is greater than both $\mu\cot(\psi_o - \delta_o)$ and $\mu\cot(\psi_o + \delta_o)$ to a value that is below both of those values. For case 1 such unloading involves a process of kink pair nucleation at the greater value and kink pair annihilation at the lesser value. In contrast, unloading of case 2 involves kink creation by the reverse of the fade out process, namely *kink fade in*. Continued unloading of case 2 then gives kink disappearance by pair annihilation.

Case 3 is the exact converse of case 2 and is represented in Fig. 6. Namely, increasing T_{app} gives kink emergence by kink fade-in but gives kink disappearance by pair annihilation. Unloading gives kink emergence by pair nucleation and disappearance by fade out.

Case 4 gives kink emergence by fade-in for both loading and unloading, and gives kink disappearance by fade out for both loading and unloading (Fig. 7).

While the above descriptions may seem somewhat exotic, these processes are in fact quite ordinary. Note also that the diagrams in Figs. 5, 6 and 7 are easily generated from a Fig. 4 type diagram by "clipping off" those portions of the Fig. 4 type diagram at which the condition $\gamma > 2/\sin^2 2\psi$ is no longer met by virtue of the inequalities that define cases 2–4.

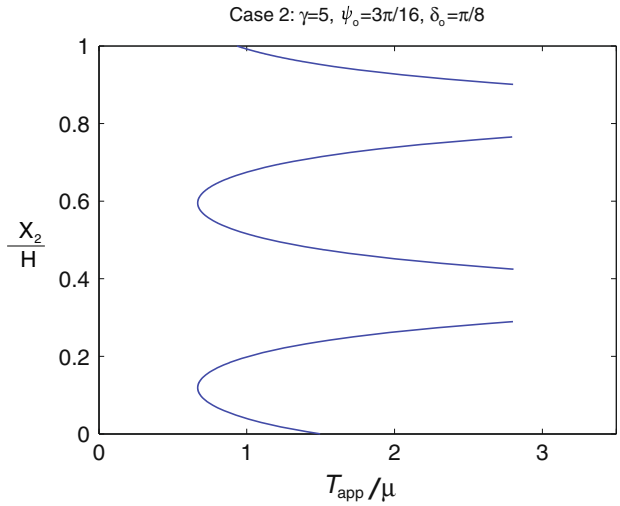

FIG. 5. Evolution of kink surfaces for case 2. Similar to case 1, kink pairs emerge at $T_{\text{app}} = \mu \cot(\psi_o + \delta_o)$ and these siblings move apart with increasing T_{app}. However, instead of pair annihilation, the kink surfaces disappear by fading out at a critical value of T_{app}

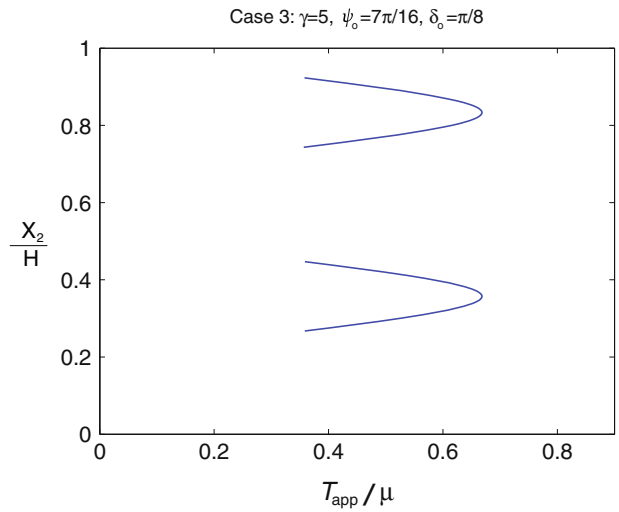

FIG. 6. Evolution of kink surfaces for case 3. Each kink emerges by fade-in but disappears by pair annihilation

While the above development applies to the specific fiber orientation field in which $\hat{\psi}(X_2)$ is given by (34), similar considerations apply to the consideration of any field $\hat{\psi}(X_2)$ for the standard reinforcing (3). Namely, locations X_2 for which $\gamma > 2/\sin^2 2\hat{\psi}(X_2)$ involve a nonmonotone shearing response so that such locations can support a kink surface. At such locations we may again define the function $\hat{T}_{\text{jcm}}(X_2)$. In general, the simple boundary value problem for the layer with fixed displacement on $X_2 = 0$ and applied shearing traction T_{app} then gives rise to the emergence, propagation and disappearance of kink surfaces as a function of the load parameter T_{app}. Any such process has a representation in terms of diagram like that in Figs. 4, 5, 6 and 7 in which the locus $T_{\text{app}} = \hat{T}_{\text{jcm}}(X_2)$ again represents how the movement

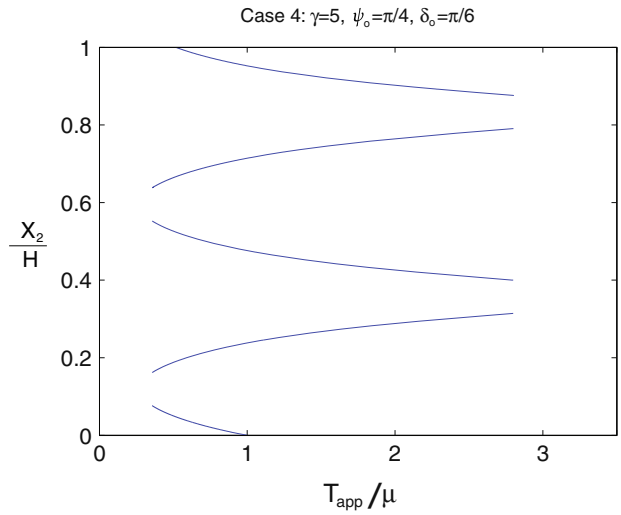

FIG. 7. Evolution of kink surfaces for case 4. Each kink emerges by fade-in and disappears by fade-out

of all kink surfaces correlates with T_{app}. Kink surface emergence may then be by any one of the three mechanisms illustrated above: pair nucleation, boundary emission, or fade-in. Kink surface disappearance may be by any one of the three converse mechanisms: pair annihilation, boundary absorption, or fade-out. All of these processes correspond graphically to a point in the (T_{app}, X_2)-plane where the vertical T_{app}-line intersects the $\hat{T}_{\text{jcm}}(X_2)$ curve at a single point in a special way. Pair emergence and annihilation correspond to an isolated point of tangential contact. Boundary emission and absorption occur if $X_2 = 0$ or $X_2 = H$. Fade-in and fade-out occurs at values X_2 where the $\hat{T}_{\text{jcm}}$-curve ceases to be defined. The more general intersection in which the intersection gives a point that is not associated with any of the above geometrical conditions corresponds to an existing kink surface in quasi-static motion. The one situation not described by this list of conditions occurs if $\hat{T}_{\text{jcm}}(X_2)$ is constant over a finite interval in X_2. Then the intersection of the T_{app}-line with the $\hat{T}_{\text{jcm}}$-curve is over a line segment. This occurs if $\hat{\psi}(X_2)$ is constant over the X_2 interval. In this case, the previously described *snap shearing* takes place for the X_2 interval in question. As is clear however from the example of the undulatory fiber direction field, any small perturbation in fiber angle orientation that eliminates such local constancy in ψ will eliminate the snap shearing by replacing it with a collection of kink pair emergence, motion, and annihilation processes.

An interesting and potentially useful converse problem also presents itself. Namely, one may seek to determine a fiber orientation distribution $\hat{\psi}(X_2)$ so as to generate a desired motion locus for the kink surfaces. For example, suppose one is given a continuous function $\hat{T}_{\text{spec}}(X_2) > 0$ that is defined for all X_2 on the full interval $0 \le X_2 \le H$. It is desired to make the spatially dependent Maxwell stress $\hat{T}_{\text{jcm}}(X_2)$ correspond to $\hat{T}_{\text{spec}}(X_2)$. For the standard reinforcing model with fixed μ and γ this is accomplished by, first, taking $\hat{\psi}(X_2) = \operatorname{arccot}(\hat{T}_{\text{spec}}(X_2)/\mu)$ and, second, requiring that γ is sufficiently large so as to give $\gamma > 2/\sin^2 2\hat{\psi}(X_2)$ for all X_2 obeying $0 \le X_2 \le H$. By this means one essentially specifies $\hat{T}_{\text{jcm}}(X_2)$ which, in particular, amounts to specifying locations and load levels at which kink pair nucleation and kink pair annihilation will take place for boundary conditions (19). If in addition it is desired to specify kink fade-in and kink fade-out then it is necessary to recall that such events are associated with the condition $\gamma = 2/\sin^2 2\psi$. This condition in turn determines two specific values of ψ which are in fact given by the bounds in (15) and (16). If we are taking positive T_{app} it is the bounds in (15) that apply in the present discussion. These bounds on ψ will in turn bound the range of values for $\hat{T}_{\text{jcm}}(X_2)$. Graphically,

the kink motion locus $T_{\rm app} = \hat{T}_{\rm jcm}(X_2)$ can be specified in a $(T_{\rm app}, X_2)$-plane by taking any continuous curve and then "clipping off" all values that are less than some predetermined number, say T_I, and similarly "clipping off" all values that are greater than some other predetermined number, say T_{II}. Under increasing $T_{\rm app}$ fade-in occurs at all the clipped points where $T_{\rm app} = T_I$ and fade-out occurs at all clipped points where $T_{\rm app} = T_{II}$. In order to make the values T_I and T_{II} correspond to the bounding angles in the inequality (15) it is then necessary to choose specific values for both μ and γ. For the standard reinforcing one finds these values to be given by

$$\mu = \sqrt{T_I T_{II}}, \quad \gamma = \frac{(T_I + T_{II})^2}{2T_I T_{II}}. \tag{35}$$

Of course if a specific value for only one clipping-off value is needed, then the other clipping-off value may be chosen as a matter of convenience. For example if only T_{II} requires assignment then T_I can be taken to be any value less than the global minimum of the function $\hat{T}_{\rm jcm}(X_2)$. This in turn relaxes the condition (35) in a fashion that could be developed in specific detail, however we feel that there is little to be gained at present in providing such elaboration.

It is also worth remarking upon that all of the considerations discussed above regarding the kink surface motion locus $T_{\rm app} = \hat{T}_{\rm jcm}(X_2)$ is in the context of material inhomogeneity due to $\psi = \hat{\psi}(X_2)$ for constant μ and γ. Even richer possibilities arise if μ and γ also display a dependence on X_2 but we do not consider such issues here.

6. Hysteretic solutions for an undulatory fiber orientation field subject to shear traction

The considerations of the previous section were for kink surfaces subject to the Maxwell condition so as to describe energy minimizing configurations. As soon as one seeks to account for hysteresis it is almost inevitable that deep questions arise as to the proper formulation of the model so as to accurately capture the underlying physics that gives rise to the hysteresis [3]. In particular, the function $\tilde{E}(\kappa, \psi)$ in (25) with κ replaced by f' naturally enters the treatment in its role as the *kink surface driving force* [4]. This is a vast subject and well beyond the scope of the present article. Instead we shall here briefly consider a simplified phenomenological view of hysteresis for the purpose of highlighting how the previous development would necessarily be modified when considering hysteresis in general.

The highly simplified approach to be considered in this section involves the a priori assignment of $T_\uparrow$ and $T_\downarrow$. A special case of this is the maximum delay convention, namely $T_\uparrow = \Gamma(k_{\max}, \psi)$ and $T_\downarrow = \Gamma(k_{\min}, \psi)$. This may be done by writing the expressions

$$T_\uparrow = T_{\rm jcm} + \Delta T_\uparrow, \qquad T_\downarrow = T_{\rm jcm} - \Delta T_\downarrow \tag{36}$$

where $\Delta T_\uparrow > 0$ and $\Delta T_\downarrow > 0$ are specified in some fashion. The specification (36) will be required to obey $\Delta T_\uparrow \leq \Gamma(k_{\max}, \psi) - T_{\rm jcm}$ and $\Delta T_\downarrow \leq T_{\rm jcm} - \Gamma(k_{\min}, \psi)$. For simplicity, let us therefore confine the brief remarks in this section to a model of the form (36) with

$$\Delta T_\uparrow = a_\uparrow(\Gamma(k_{\max}, \psi) - T_{\rm jcm}), \qquad \Delta T_\downarrow = a_\downarrow(T_{\rm jcm} - \Gamma(k_{\min}, \psi)) \tag{37}$$

where the multipliers $a_\uparrow$ and $a_\downarrow$ *are constants* obeying $0 \leq a_\uparrow \leq 1$ and $0 \leq a_\downarrow \leq 1$. Thus $a_\uparrow = a_\downarrow = 1$ is the maximum delay convention and $a_\uparrow = a_\downarrow = 0$ is the Maxwell convention. Clearly, a more fundamental perspective would connect the determination of the multipliers $a_\uparrow$ and $a_\downarrow$ to the physical processes giving rise to the dissipation. The simple model here is sufficient, however, for a basic illustration, by means of two examples, of how hysteresis can modify the most basic aspects of kink surface emergence and disappearance.

The first example is associated with case 2 when there is no hysteresis. Thus the off-axis shear response is monotone at some values of X_2 and nonmonotone for the remaining X_2. Where the off-axis shear response is monotone, the value of f' only depends upon $T_{\rm app}$ and, in particular, is independent of the

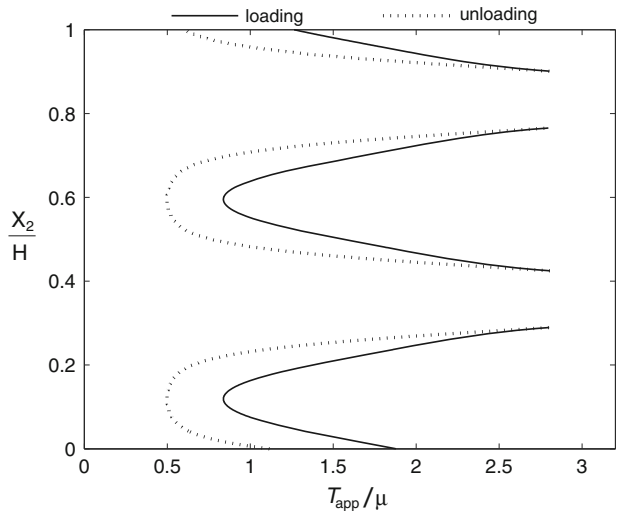

FIG. 8. A hysteresis delay in the jump between branches of the off-axis shear response [e.g., $a_\uparrow = a_\downarrow = 0.8$ in (37)] causes the kink surfaces to trace out different paths for increasing and decreasing T_{app}. Here the fiber orientation field and γ are identical to the values for Fig. 5

direction of loading. In contrast, at each X_2 where the response is nonmonotone, there is a range of T_{app} associated with hysteresis. Figure 8 displays a diagram of T_{app} versus kink surface X_2 locations for the same material parameters and fiber orientation field as that which generated Fig. 5 in the absence of hysteresis. Similar to Fig. 5, loading involves pair creation and fade-out, whereas unloading involves fade-in and pair annihilation. The curves in Fig. 8 enclose the hysteresis region, and this hysteresis region contains the original Fig. 5 curves.

The second example corresponds to case 1 when there is no hysteresis, and is chosen so that certain X_2 are associated with region III in Fig. 3. By virtue of the correspondence with case 1, every point in the layer involves nonmonotone response, and so all locations exhibit hysteresis in this example. At those X_2 locations corresponding to region III in Fig. 3, one may take $a_\downarrow$ sufficiently large so that the shearing is still on the secondary branch for $T_{\text{app}} = 0$. Figure 9 provides an example where this is the case for some, but not all X_2. Thus in the example of Fig. 9, loading so as to put all shears on the secondary branch, followed by unloading back to $T_{\text{app}} = 0$ results in some X_2 locations with shearing on the primary branch, and hence $f' = 0$ at those locations. However at the remaining X_2 values one finds $f' > 0$ because those shears remain on the secondary branch at $T_{\text{app}} = 0$. Thus the unloaded state will not only have strains on the secondary branch at various X_2, but will also have kink surfaces in the fully unloaded zero stress configuration. The positive shears give rise to a residual deformation of the top surface after complete load removal.

7. More general boundary conditions for rectilinear shear

The consideration of the previous sections have strong consequences for the solution of more difficult boundary value problems. It is the purpose of this section to indicate some of these consequences. Let us first remark on the boundary value problem considered in the previous two sections, namely a finite thickness layer of infinite extent subject to fixed displacement on one side and, on the other side, subject to zero normal traction and uniform shear traction. We solved this boundary value problem by considering the rectilinear shear deformation field, choosing the rectilinear shear $f(X_2)$ and the Lagrange multiplier

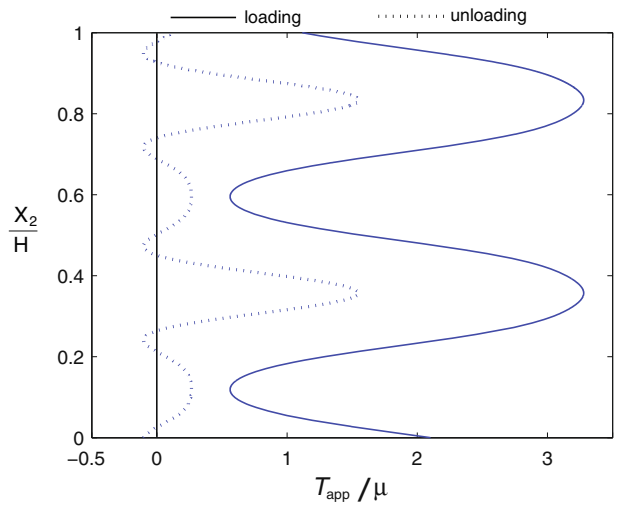

FIG. 9. The delay in jump condition shifts the plot, $T_{\rm app}/\mu$ versus X_2/H, to the right and left respectively for loading and unloading. The plots also alter their overall shape. Here we take $\psi_o = \pi/4$, $\delta_o = \pi/8$, $\gamma = 10$, $\omega = 4.2\pi$, and $a_\uparrow = a_\downarrow = 0.8$. If $\{\gamma,\ \psi\}$ corresponds to region III of Fig. 3, then $T_{\rm app} = 0$ is consistent with shear values $\kappa > 0$ on the secondary branch. For the present example, this occurs for certain intervals in X_2 so that there is a residual displacement of the top layer when the load is removed

$p(X_2)$ so as to give a Cauchy stress $\mathbf{T}$ of the form (33). Such a stress field would usually be viewed as trivial, since each term in the Cartesian representation of the equilibrium equation div$\mathbf{T} = \mathbf{0}$ is found to vanish identically.

A situation in which this is not the case occurs for the type of boundary value problem that is usually associated with the rectilinear shear displacement field. Namely, in the previous two sections we were led to consider the rectilinear shear displacement field not because the specified boundary conditions (19) were "difficult", but rather because the material was spatially inhomogeneous by virtue of $\psi = \hat{\psi}(X_2)$. An alternative situation in which one is motivated to consider the rectilinear shear deformation is for homogeneous materials subject to relatively more difficult boundary conditions. This is the situation examined in [21] where a similar type of layer is under consideration, although attention in [21] is restricted to a spatially constant fiber orientation field.

Let us therefore generalize the traction boundary conditions that we wish to consider on the top surface from (19) to

$$\mathbf{t} = T_{\rm app}\mathbf{e}_1 + (B_{\rm app}x_1 + C_{\rm app})\mathbf{e}_2 \quad \text{on} \quad X_2 = H. \tag{38}$$

Here the constants $B_{\rm app}$ and $C_{\rm app}$ join $T_{\rm app}$ as load parameters, all of which can be varied in a quasi-static fashion. Our continued interest concerns the emergence, motion and disappearance of kink surfaces in the layer as these load parameters are varied. In this case, the spatial variation of the boundary condition term $B_{\rm app}x_1$ causes the stress field to be more complicated than the simple form (33) and the question arises as to how to describe the effect that this has on the behavior of any kink surfaces.

For the problem stated above with boundary condition (38) we continue to seek solutions involving the rectilinear shear displacement field (30) in which $f(X_2)$ is smooth except at certain locations where f' is discontinuous. Such locations of course correspond to kink surfaces. In general for the deformation field (30), the Cauchy stress is of the form (9) with T_{12} given by (10) and T_{22} given by (11) under the replacement $\kappa \to f'$ indicated previously in (31). The equilibrium equation div$\mathbf{T} = \mathbf{0}$ may therefore be written as

$$-\frac{\partial p}{\partial x_1}+\frac{\partial}{\partial x_2}\left(\Gamma(f'(x_2),\hat{\psi}(x_2)\right)=0, \tag{39}$$

$$\frac{\partial T_{22}}{\partial x_2}=0, \tag{40}$$

$$-\frac{\partial p}{\partial x_3}=0, \tag{41}$$

where we have used $X_2=x_2$ in (39). Now (41) gives $p=p(x_1,x_2)$ whereupon (40) in conjunction with (11) and (31) yields

$$p(x_1,x_2)=\mu+\mu\gamma\sin^2\psi W'_{fib}\left(1-2f'\sin\psi\cos\psi+(f')^2\sin^2\psi\right)+q(x_1), \tag{42}$$

with $\psi=\hat{\psi}(x_2)$ and $f'=f'(x_2)$. It then follows from (39) that

$$q(x_1)=c_1x_1+c_2, \tag{43}$$

and it further follows that

$$T_{22}=-q(x_1)=-c_1x_1-c_2. \tag{44}$$

This disposes of (40) and (41) whereas (39) reduces to

$$\Gamma(f'(x_2),\hat{\psi}(x_2))=c_1x_2+c_3. \tag{45}$$

The boundary conditions have yet to be considered in this development. In addition, in the event that there are kink surfaces it follows that the above equations hold in each layer between any two such kink surfaces. In other words, while c_1, c_2, and c_3 are constant in each layer, the mathematical integration procedure in principle permits these constants to take on different values in the different layers. However, traction continuity across the kink surfaces requires that the same values c_1, c_2, and c_3 obtain throughout. Thus (44) and (45) must hold throughout the whole layer for common values of the constants c_1, c_2, and c_3 even in the presence of kink surfaces.

It now follows from (44) in conjunction with the normal traction portion of the boundary condition (38) that $c_1=-B_{\rm app}$ and $c_2=-C_{\rm app}$. It then follows from (44) in conjunction with the shear traction portion of the boundary condition (38) that $T_{\rm app}=-B_{\rm app}H+c_3$ so that $c_3=B_{\rm app}H+T_{\rm app}$. Hence (45) becomes

$$\Gamma(f'(X_2),\hat{\psi}(X_2))=-B_{\rm app}X_2+B_{\rm app}H+T_{\rm app} \tag{46}$$

where we have again made use of $x_2=X_2$. This is now an equation to be solved for $f'(X_2)$ both when kink surfaces are absent and when kink surfaces are present. The function $f(X_2)$ again follows by integration using $f(0)=0$ and continuity of f across any kink surface.

Observe that (46) reduces to (32) when $B_{\rm app}=0$. Note also that $C_{\rm app}$ does not appear in the governing equation (46). This could have been anticipated on the basis of the fact that $C_{\rm app}$ appears in (38) in such a way that it can always be accommodated by changing the ambient value of the overall hydrostatic pressure field.

In particular (46) applies for the standard reinforcing with $\gamma<2$ in which case the previously introduced inverse function notation $\Lambda(T,\psi)$ allows us write

$$f'(X_2)=\Lambda(-B_{\rm app}X_2+B_{\rm app}H+T_{\rm app},\hat{\psi}(X_2)). \tag{47}$$

This includes the special case $\gamma=0$ which corresponds to a neo-Hookean material. For $\gamma=0$ it follows that $\Lambda(T,\psi)$ is independent of ψ. In particular $\Lambda(T,\psi)=T/\mu$ so that (47) gives $f'(X_2)=-(B_{\rm app}/\mu)(X_2-H)+T_{\rm app}/\mu$ and hence $f(X_2)=-(B_{\rm app}/2\mu)X_2^2+(B_{\rm app}H+T_{\rm app})X_2/\mu$. In particular, the lateral displacement of the top surface is $f(H)=B_{\rm app}H^2/2\mu+T_{\rm app}H/\mu$ for the neo-Hookean material which clearly shows how this simple solution is dependent on the quasi-static load parameters $B_{\rm app}$ and $T_{\rm app}$.

If $\Gamma(\kappa, \hat{\psi}(X_2))$ is nonmonotone for certain X_2 then all of the same issues arise as previously considered in the development of Sects. 5 and 6 for the simpler boundary conditions (19). For the more general boundary conditions (38) the same type of arguments and remedies apply. In particular, energy minimizing solutions involve kink surfaces in which the value of T_{12} is equal to the local value of the Maxwell stress on each side of the kink surface. Hence $f'(X_2)$ is formally given by

$$f'(X_2) = \Lambda_{\rm jcm}(-B_{\rm app}X_2 + B_{\rm app}H + T_{\rm app}, \hat{\psi}(X_2)) \tag{48}$$

and X_2 values that give the location of a kink surface are roots to the equation

$$-B_{\rm app}X_2 + B_{\rm app}H + T_{\rm app} = \hat{T}_{\rm jcm}(X_2) \tag{49}$$

where $\hat{T}_{\rm jcm}(X_2)$ is the same function that played so central a role in the development of Sect. 5.

Equation (49) permits one to determine the appearance, motion, and disappearance of kink surfaces by a similar reasoning as that considered in Sect. 5 for the simpler boundary condition (19) and which led to the graphical representations in Figs. 4, 5, 6 and 7. Now, however, let us regard the plane in these figures not as a $(T_{\rm app}, X_2)$-plane of values but rather as a (T_{12}, X_2)-plane of values. For the previous analysis this distinction is moot since $T_{12} \equiv T_{\rm app}$ for the solutions considered in Sects. 5 and 6. However for the boundary condition (38) it is now the case that $T_{12} = T_{\rm app} + B_{\rm app}(H - X_2)$ which generates a line in the (T_{12}, X_2)-plane that is vertical only if $B_{\rm app} = 0$. Equation (49) motivates the consideration of how this line intersects the curve $T_{12} = \hat{T}_{\rm jcm}(X_2)$. In particular, the type of intersections enumerated previously continue to be associated with the same type of kink surface phenomena. Namely, the following specialized intersections have the associated interpretation in terms of kink appearance or disappearance:

- Single point tangential intersection implies kink-pair creation or annihilation.
- Single point transverse intersection at either $X_2 = 0$ or $X_2 = H$ implies boundary emission or absorption.
- Single point transverse intersection that coincides with an internal endpoint to the $\hat{T}_{\rm jcm}$-curve implies fade-in or fade-out.
- Intersection over an interval of X_2-values implies snap shifting.

On the other hand, the more generic intersection possibility, namely:

- Single point transverse intersection on $0 < X_2 < H$ that does not coincide with an internal endpoint to the $\hat{T}_{\rm jcm}$-curve implies a preexisting kink surface.

Consider once again the case $\psi = \psi_o$ a constant for the standard reinforcing with $\gamma > 2/\sin^2 2\psi_o$ so that the locus $\hat{T}_{\rm jcm}(X_2)$ is independent of X_2 and hence gives the vertical line $\hat{T}_{\rm jcm} = \mu \cot \psi_o$ in the (T_{12}, X_2)-plane. For the boundary condition (19) considered in Sect. 5 the graphical intersection only occurs for $T_{\rm app} = \mu \cot \psi_o$ and this intersection occurs over the full interval of X_2-values $0 \le X_2 \le H$. Thus for quasi-statically increasing $T_{\rm app}$ there is snap shift over the whole layer at this special value of $T_{\rm app}$. Now, suppose that the boundary condition (19) is replaced by the more general (38) with $T_{\rm app} = 0$, $C_{\rm app} = 0$, and $B_{\rm app}$ monotonically increasing from zero. In this case, there is no graphical intersection until $B_{\rm app} = (\mu/H)\cot \psi_o$ and this intersection corresponds to the boundary emission of a kink surface at $X_2 = 0$. As is shown by the graphical construction in Fig. 10, continued increase in $B_{\rm app}$ causes the intersection value of X_2 to increase to $X_2 = H - (\mu/B_{\rm app})\cot \psi_o$. Indeed this equation represents the trajectory of the kink surface in a $(B_{\rm app}, X_2)$-plane of values, shown also in Fig. 10, in a similar way that Figs. 4, 5, 6, 7, 8 and 9 represented kink surface location versus the different quasi-static load parameter $T_{\rm app}$.

Now let us consider an example involving $\psi = \hat{\psi}(X_2)$ so that $\hat{T}_{\rm jcm}(X_2)$ is no longer constant. In view of the correspondence between $\psi = \hat{\psi}(X_2)$ and $\hat{T}_{\rm jcm}(X_2)$ we may alternatively consider specified functions

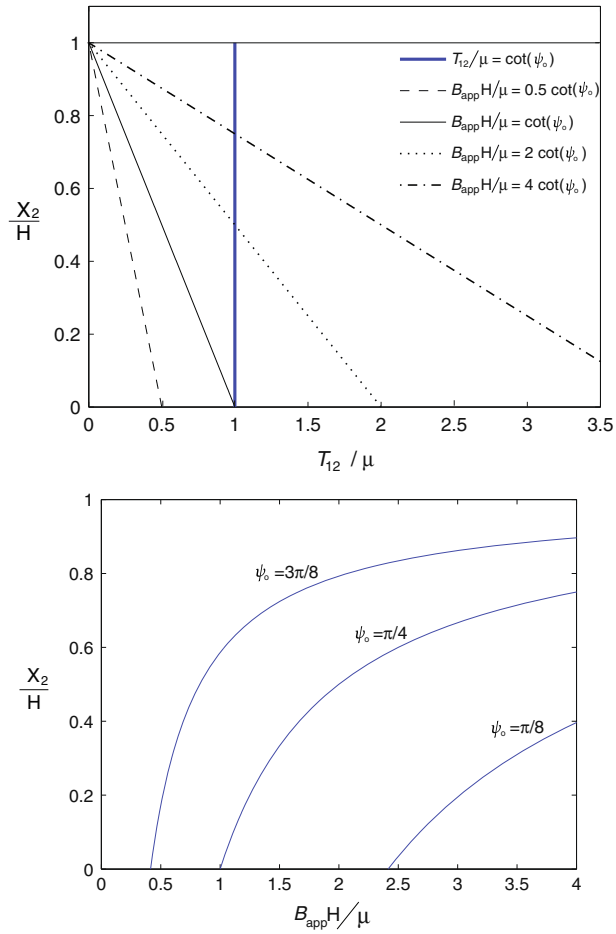

FIG. 10. Appearance and movement of a kink surface under the traction boundary conditions (38) with $T_{\rm app} = 0$. *Above* the intersection between the vertical line segment $T_{12}/\mu = \cot\psi_o$ and the line $T_{12}/\mu = B_{\rm app}H/\mu(1 - X_2/H)$ gives the kink surface location as a function of $B_{\rm app}$. *Below* the kink surface in a $(B_{\rm app}H/\mu, X_2/H)$—plane is plotted for $\psi_o = \pi/8$, $\pi/4$, and $3\pi/8$

$\hat{T}_{\rm jcm}(X_2)$. Take for example a function $\hat{T}_{\rm jcm}(X_2)$ that is given as follows:

$$\hat{T}_{\rm jcm}(X_2) = \begin{cases} T_1, & \text{if} \quad 0 < X_2 < \frac{1}{3}H, \\ \frac{1}{2}(T_1 + T_2) + \frac{1}{2}(T_2 - T_1)\sin(\frac{3\pi}{2H}(2X_2 - H)), & \text{if} \quad \frac{1}{3}H < X_2 < \frac{2}{3}H, \\ T_2, & \text{if} \quad \frac{2}{3}H < X_2 < H, \end{cases} \tag{50}$$

where $T_1 > T_2$ are positive constants. Let us now compare the quasi-static layer response for two cases of (38), the first being a case with $B_{\rm app} = 0$ and increasing $T_{\rm app}$ and the second being a case with $T_{\rm app} = 0$ and increasing $B_{\rm app}$.

For $B_{\rm app} = 0$ and $T_{\rm app}$ increasing from zero the boundary condition is equivalent to that considered in Sect. 5 in connection with (19). The associated kink surface motion locus in the $(T_{\rm app}, X_2)$-plane follows directly from $\hat{T}_{\rm jcm}(X_2)$ and is shown in Fig. 11. In this case, it follows that the response is everywhere confined to the primary branch of the local off-axis shearing response for $0 \le T_{\rm app} < T_2$. At $T_{\rm app} = T_2$ there is a snap shearing of the top one third of the layer. After this snapping, a single kink surface moves

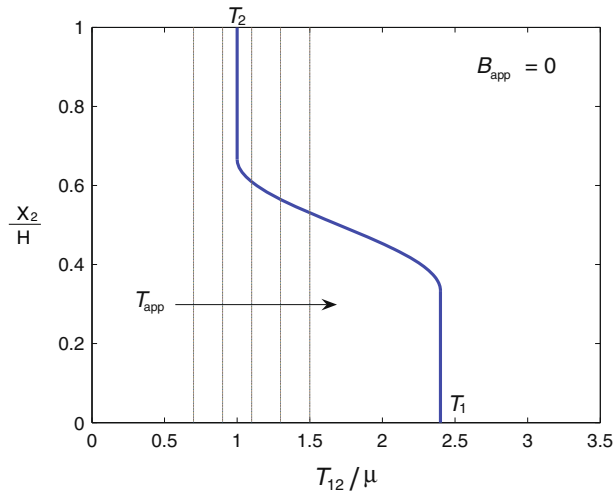

FIG. 11. Kink surface creation and movement under various boundary conditions. The function $\hat{T}_{\rm jcm}(X_2)$ is given by (50). $B_{\rm app} = 0$ and $T_{\rm app}$ is increasing. The intersection of $T_{12} = T_{\rm app}$ with the curve given by (50) corresponds to the kink surface. Here $T_2 = 1.0\mu$ and $T_1 = 2.4\mu$

within the layer as $T_{\rm app}$ increases through the interval $T_2 < T_{\rm app} < T_1$. This kink surface appears at $X_2 = 2H/3$, which is at the bottom of the snapped region, at the snapping load $T_{\rm app} = T_2$. Increasing $T_{\rm app}$ causes this kink surface to descend through the middle third of the overall layer. At $T_{\rm app} = T_1$ this kink surface finds itself at $X_2 = H/3$ whereupon the top two thirds of the layer has shears on the secondary branch of the local off-axis shearing response, while the bottom one third of the layer still has shears on the local primary branch. Then as $T_{\rm app}$ increases through the value T_1 there is a another snap shearing, this time on the bottom one third of the layer, so that it too will subsequently have shears on the secondary branch.

The other loading case, that in which $T_{\rm app} = 0$ and $B_{\rm app}$ increases from zero, involves a quite different developmental evolution for the kink surfaces. However, like the previous case, sufficiently small load parameter (now $B_{\rm app}$) gives a shearing response that is everywhere associated with the primary branch of the local off-axis response. To discuss this case note that the graphical construction involves the line $T_{12} = B_{\rm app}(H - X_2)$ which always includes the point $(T_{12}, X_2) = (0, H)$. This line is vertical for $B_{\rm app} = 0$ and it "swings up" as $B_{\rm app}$ increases. The nature and ordering of the intersections depends on the relation between T_1 and T_2. Let us suppose that $1.54T_2 < T_1 < 2.85T_2$. Then, as the $B_{\rm app}$-line swings up, there are three values of $B_{\rm app}$ that give special intersections with the $\hat{T}_{\rm jcm}$-curve as shown in Fig. 12. The first value, say B_1, is that which causes the intersection to occur at the point $(T_{12}, X_2) = (T_1, 0)$. The second, say B_2, gives the unique tangential intersection that occurs on the interval $H/2 < X_2 < 2H/3$. The third, say B_3, gives the unique tangential intersection that occurs on the interval $H/3 < X_2 < H/2$. These values are ordered $0 < B_1 < B_2 < B_3$. It then follows that kink surfaces appear and disappear as follows. As $B_{\rm app}$ increases from 0 to B_1 the shears are everywhere on the local primary branch and there are no kink surfaces. A kink surface is emitted from the boundary $X_2 = 0$ when $B_{\rm app} = B_1$ and this kink surface moves into the interior by increasing its X_2 location as $B_{\rm app}$ increases over the interval $B_1 < B_{\rm app} < B_3$. In addition, at $B_{\rm app} = B_2 < B_3$ a pair of kinks are nucleated at the X_2 value between $X_2 = H/2$ and $X_2 = 2H/3$ which provides the tangential contact point of the construction for $B_{\rm app} = B_2$. These internally nucleated kinks move in opposite directions as $B_{\rm app}$ increases over the interval $B_2 < B_{\rm app} < B_3$. At $B_{\rm app} = B_3$ the sibling kink that was moving downward encounters the kink that had been emitted from the lower boundary, and these two kinks annihilate. Then for $B_{\rm app} > B_3$ the remaining upward moving

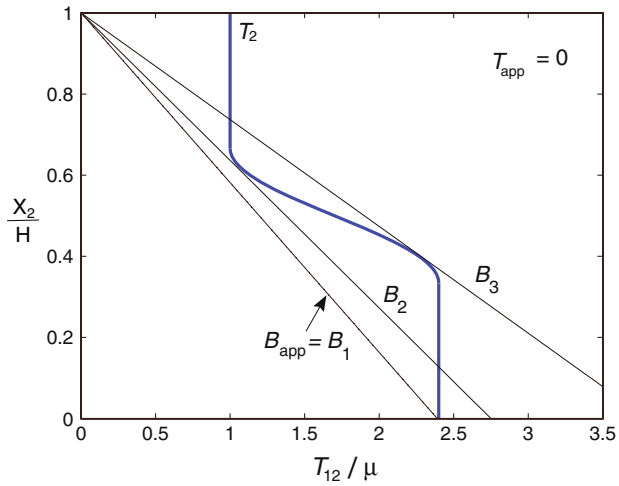

FIG. 12. Similar to Fig. 11, but the parameters in the traction boundary condition (38) now have $T_{\rm app} = 0$. As $B_{\rm app}$ increases, the line $T_{12}/\mu = B_{\rm app}H/\mu(1 - X_2/H)$ meets with the curve (50) at $B_{\rm app} = B_1$, the first tangential intersection occurs at $B_{\rm app} = B_2$, and the second tangential intersection occurs at $B_{\rm app} = B_3$

sibling kink continues to move toward the upper boundary $X_2 = H$, approaching this boundary in an asymptotic fashion as $B_{\rm app} \to \infty$.

The above example did not involve fade-in or fade-out processes since the function $\hat{T}_{\rm jcm}(X_2)$ was defined for all X_2 in the layer. Clearly, however, the same graphical methodology applies in the event that $\hat{T}_{\rm jcm}(X_2)$ is only defined for a restricted range of values in the layer. For boundary conditions (19) such functions $\hat{T}_{\rm jcm}(X_2)$ gave kink fade-in and fade-out as described previously with respect to Figs. 5, 6 and 7. Such functions $\hat{T}_{\rm jcm}(X_2)$ will continue to give rise to kink fade-in and fade-out for the more general boundary conditions (38).

It is also to be remarked that although the just completed example involved two cases, one with $B_{\rm app} = 0$ and the other with $T_{\rm app} = 0$, one can certainly investigate the simultaneous change in both parameters by a similar graphical construction in the (T_{12}, X_2)-plane.

For example we may imagine $T_{\rm app} = \hat{T}_{\rm app}(t)$ and $B_{\rm app} = \hat{B}_{\rm app}(t)$ which regards the quasi-static load functions to be explicit functions of a time parameter t. Consider for example $\hat{T}_{\rm app}(t) = \tau_{\rm app}t$ and $\hat{B}_{\rm app}(t) = \beta_{\rm app}t$ with constants $\tau_{\rm app} \geq 0$ and $\beta_{\rm app} \geq 0$. For the sake of a simple illustration, let us return again to the constant orientation example $\psi = \psi_o$ with $\gamma > 2/\sin^2 2\psi_o$ so that $\hat{T}_{\rm jcm}(X_2) = \mu \cot\psi_o$ is independent of X_2. Since we have explicitly introduced a time t let us also introduce an explicit kink surface location function s which therefore is to be regarded as a function of time, i.e., $s = s(t)$. The function $s(t)$ is undefined if there are no kink surfaces and is multi-valued if there are multiple kink surfaces. Then (49) with $\psi = \psi_o$ gives

$$-\beta_{\rm app}ts(t) + \beta_{\rm app}tH + \tau_{\rm app}t = \mu\cot\psi_o \tag{51}$$

from which it follows that a single kink surface is emitted from $X_2 = 0$ at

$$t_{\rm emit} = \left(\frac{\mu}{\tau_{\rm app} + \beta_{\rm app}H}\right)\cot\psi_o. \tag{52}$$

This kink surface then travels across the layer before being absorbed on $X_2 = H$ at

$$t_{\rm absorb} = \frac{\mu}{\tau_{\rm app}}\cot\psi_o. \tag{53}$$

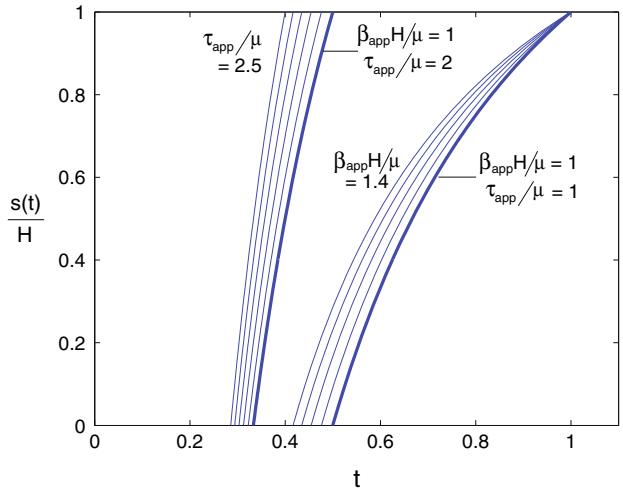

FIG. 13. The time dependent movement of kink surfaces. $\hat{T}_{\rm jcm}(X_2)/\mu = \cot(\pi/4)$. The functions $s(t)/H$ are plotted for various values of the relevant nondimensionalized parameters. The left series of curves is generated by fixing $\beta_{\rm app}H/\mu = 1$ and taking $\tau_{\rm app}$ as 2.0–2.5. The right series of curves generated by fixing $\tau_{\rm app}/\mu = 1$ and taking $\beta_{\rm app}H/\mu$ as 1.0–1.4

During this transit the kink surface location is given by

$$s(t) = H + \frac{\tau_{\rm app}}{\beta_{\rm app}} - \frac{\mu \cot\psi_o}{\beta_{\rm app} t}, \qquad t_{\rm emit} \le t \le t_{\rm absorb}. \tag{54}$$

The function $s(t)$ is displayed in Fig. 13 for various $\tau_{\rm app}$ and $\beta_{\rm app}$. Such a trajectory for $\tau_{\rm app} \to 0$ at fixed $\beta_{\rm app} > 0$ would correspond to the Fig. 10 diagram in which $T_{\rm app} = 0$. The converse limit of $\beta_{\rm app} \to 0$ at fixed $\tau_{\rm app} > 0$ gives an undefined $s(t)$ wherein the interval $t_{\rm emit} \le t \le t_{\rm absorb}$ collapses to the single instant $t = t_{\rm absorb}$ which is indicative of the sudden snap shear that occurs in the case $B_{\rm app} = 0$.

A similar set of curves can be constructed with $\hat{T}_{\rm app}(t) = \tau_{\rm app} t$ and $\hat{B}_{\rm app}(t) = \beta_{\rm app} t$ for *any* orientation distribution $\psi = \hat{\psi}(X_2)$. In particular, for the orientation distribution that results in $\hat{T}_{\rm jcm}(X_2)$ given by (50) one obtains the curves in Fig. 14. In this case, $s(t)$ may be multi-valued and the correspondence with the respective previously considered separate cases $B_{\rm app} = 0$ and $T_{\rm app} = 0$ follow for the separate limits $\beta_{\rm app} \to 0$ at fixed $\tau_{\rm app} > 0$ and $\tau_{\rm app} \to 0$ at fixed $\beta_{\rm app} > 0$ respectively. For the general case $\tau_{\rm app} > 0$ and $\beta_{\rm app} > 0$ the solution will generally involve kink surface creation via both boundary emission at $X_2 = 0$ and pair nucleation on $H/2 < X_2 < 2H/3$. However, the order in which these events occur will depend on the various parameters in the problem. Kink surface disappearance will generally involve both pair annihilation on $H/3 < X_2 < H/2$ and boundary absorption at $X_2 = H$ where the ordering is again parameter dependent.

8. More general boundary value problems

These examples show general features of boundary value problems for transversely isotropic hyperelastic materials for which shearing occurs in fiber containing planes. Specifically, we have shown that if the constitutive response for the off-axis shearing stress is nonmonotonic with respect to the amount of shear, and if in addition the applied loading exceeds threshold values determined by the off axis shearing response, then the resulting deformation field will include internal kink surfaces. These surfaces develop by a variety of mechanisms that we have described here in terms of boundary emission, pair nucleation, and fade-in processes. Each of these has a counterpart process that results in the disappearance of a kink

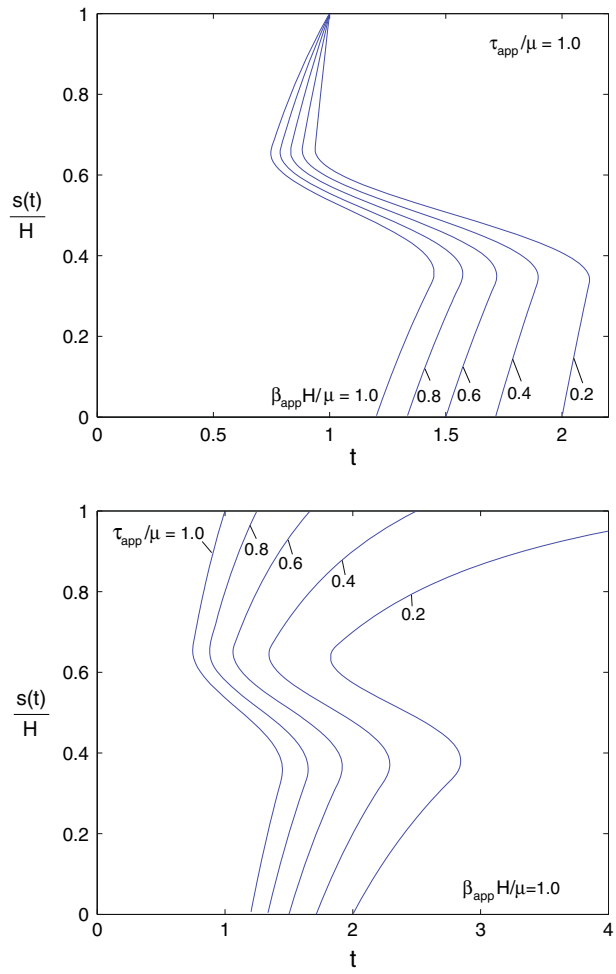

FIG. 14. Similar to Fig. 13, but now $\hat{T}_{\rm jcm}(X_2)$ is given by (50). In this case, depending on the values of $\tau_{\rm app}/\mu$ and $\beta_{\rm app}H/\mu$, the appearance of a kink surface is either by kink nucleation or by boundary emission. Kink surfaces disappear either by pair annihilation or by being absorbed at the boundary

surface. In particular, both the boundary value problem for rectilinear shear considered in [21] and the boundary value problem for azimuthal shear considered in [12] give rise to such kink surfaces. We now comment upon the connections of the present work to each of these in turn, beginning with [21].

Since both the problem considered here and that considered in [21] involve rectilinear shear, various mathematical equations in the two treatments can be rendered equivalent by algebraic manipulation. In particular, (46) corresponds to (30) of [21]. The boundary conditions associated with the two treatments are, however, a little different. The problem considered in [21] would correspond in our notation to requiring $f(0) = 0$ and $f(H) = 0$. One could therefore connect the two treatments by regarding our $B_{\rm app}$ as a specified quantity and then seeking the value $T_{\rm app}$ so as to give $f(H) = 0$. Indeed the condition (56) in [21] can be interpreted in such a fashion. In addition, the problem considered in [21] involves a spatially uniform fiber direction and so would correspond to the special case $\psi = \psi_o$ considered here. Finally, the development in [21] does not specifically restrict attention to kink surfaces on which the shear stress is restricted to the Maxwell value. Instead, the development in [21] is more in keeping with the maximum delay convention. It should therefore be the case that the treatment in [21] would also find

that the development of kink surfaces requires $\gamma > 2$. In addition, for a phenomena like the permanent deformation after unloading obtained here in Sect. 6, any such associated anomalous phenomena should manifest itself in [21] if $\gamma > 8$. The treatment of [21] instead finds that kink surfaces occur if $\gamma > 4$ (see the discussion before (66) in [21]), and that the threshold for an additional breakdown in solutions takes place at $\gamma = 16$ (see the discussion after (53) in [21]). The factor of two difference between these threshold values compared to those obtained in [23], and confirmed by us here, is resolved when one corrects for a factor of two that was dropped in going from (4) to (18), (19), and (22) of [21]. If this factor is restored, which formally causes $\gamma \to 2\gamma$ from Sect. 3 onward in [21], then the expected consistency in threshold values for the reinforcing parameter γ is restored with respect to [21,23] and the present paper.

The azimuthal shearing problem considered in [12] uses cylindrical polar coordinates (R, Θ, Z) and (r, θ, z) in the reference and deformed configurations, respectively, and, making allowance for notational differences, involves taking $\mathbf{A} = -\sin\psi \mathbf{e}_R + \cos\psi \mathbf{e}_\Theta$ with $\psi = \hat{\psi}(R)$. The deformation is given by

$$r = R, \qquad \theta = \Theta + g(R), \quad z = Z. \tag{55}$$

It follows that $\mathbf{F} = \mathbf{I} + Rg'(R)\mathbf{e}_\theta \otimes \mathbf{e}_R$ so that this deformation too is locally a simple shear. In this case, one finds that integration of the equilibrium equations determines the hydrostatic pressure p up to a single constant, and also leads to the condition

$$\Gamma(Rg'(R), \hat{\psi}(R)) = \frac{D_{\rm app}}{R^2}. \tag{56}$$

Here $D_{\rm app}$ is a constant of integration. A standard domain associated with the deformation (55) is a hollow tube of inner radius R_i and outer radius R_o such that the inner boundary is held fixed. The deformation could then be generated by applying a uniform $T_{R\Theta}$ shear traction on the outer boundary in which case $D_{\rm app}$ can be directly related to the value of this applied traction (see (42) and (43) of [12]). A number of such examples are developed in [12] so as to give energy minimizing solutions as a function of the value of the applied shear traction. This includes an example in which the equivalent of $\hat{\psi}(R)$ is monotonic in R such that $\psi = \pi/4$ at an internal value $\bar{R}_{\pi/4}$ obeying $R_i < \bar{R}_{\pi/4} < R_o$. Then for $\gamma > 2$ there will be an interval in R, with $\bar{R}_{\pi/4}$ in the interval interior, for which $\Gamma(\kappa, \hat{\psi}(R))$ is nonmonotonic in κ. On this interval one may define $\hat{T}_{\rm jcm}(R)$ in the same manner as for the rectilinear shear problem. Depending on the parameters in the problem, the interval of definition for the function $\hat{T}_{\rm jcm}(R)$ could be confined strictly to the interior of the tube (if γ is not too much bigger than 2), or it could extend so as to encompass $R = R_i$, $R = R_o$ or both values. It is then clear that all of the kink surface nucleation and disappearance phenomena discussed here in the context of rectilinear shear (pair nucleation and annihilation, boundary emission and absorption, fade-in and fade-out, snap-shearing) can be similarly obtained in the context of azimuthal shear by determining the graphical intersections associated with the equation $\hat{T}_{\rm jcm}(R) = D_{\rm app}/R^2$ under increasing $D_{\rm app}$. In particular, one example that is developed in detail in [12] can be viewed in this fashion, where it is shown how a kink surface fades-in at one value of load, and subsequently increases its radial location as the load increases, before fading out at some final value of load while still in the interior of the tube.

A similar treatment applies to the axial shearing deformation of a hollow circular tube with a fixed inner boundary. This is also described by means of cylindrical polar coordinates (R, Θ, Z) and (r, θ, z) in the reference and deformed configurations, respectively. The axial shearing deformation is then given by

$$r = R, \qquad \theta = \Theta, \qquad z = Z + h(R). \tag{57}$$

Thus for this deformation it follows that $\mathbf{F} = \mathbf{I} + h'(R)\mathbf{e}_z \otimes \mathbf{e}_R$. Suppose now that $\mathbf{A} = -\sin\psi \mathbf{e}_R + \cos\psi \mathbf{e}_Z$ with $\psi = \hat{\psi}(R)$. Then integration of the equations of equilibrium while enforcing a requirement of traction continuity across all kink surfaces proceeds in a manner that can be viewed as the analogous polar coordinate version of the previous Cartesian coordinate development from (39) to (46). This determines p to within a single constant and also gives

$$\Gamma(h'(R), \hat{\psi}(R)) = E_{\text{app}} R + \frac{F_{\text{app}}}{R} \tag{58}$$

for the determination of $h'(R)$. The constants E_{app} and F_{app} arise originally as integration constants. However, they may subsequently be viewed as quasi-static load parameters. In analogy with the rectilinear shear problem, the parameter E_{app} can be associated with a constant gradient in applied normal traction on the tube's outer boundary whereas the value F_{app} can be associated with a constant axial shear traction on this same boundary. It therefore follows that entirely analogous kink surface emergence and disappearance phenomena also apply in the case of the axial shearing deformation (57).

References

1. Abeyaratne, R.C., Knowles, J.K.: Discontinuous deformation gradients in plane finite elastostatics of incompressible materials. J. Elast. **10**, 255–293 (1980)
2. Abeyaratne, R.C.: Discontinuous deformation gradients in the finite twisting of an incompressible elastic tube. J. Elast. **11**, 43–80 (1981)
3. Abeyaratne, R.C., Knowles, J.K.: On the dissipative response due discontinuous strains in bars of unstable elastic material. Int. J. Solids Struct. **24**, 1021–1044 (1988)
4. Abeyaratne, R., Knowles, J.K.: Evolution of phase transitions: a continuum theory. Cambridge University Press, London (2006)
5. Atkin, R.J., Fox, N.: An Introduction to the Theory of Elasticity. Longman, London (1980)
6. Bhattacharya, K.: Phase boundary propagation in heterogeneous bodies. Proc. R. Soc. London A **455**, 757–766 (1999)
7. Ericksen, J.L.: Equilibrium of bars. J. Elast. **5**, 191–201 (1975)
8. Fu, Y.B., Zhang, Y.T.: Continuum mechanical modeling of kink-band formation in fibre-reinforced composites. Int. J. Solids Struct. **43**, 3306–3323 (2006)
9. Gao, D.Y., Ogden, R.W.: Closed-form solutions, extremality and nonsmoothness criteria in a large deformation elasticity problem. ZAMP **59**, 498–517 (2008)
10. Gasser, T.C., Ogden, R.W., Holzapfel, G.A.: Hyperelastic modeling of arterial layers with distributed collagen fibre orienations. Proc. R. Soc. Interface **3**, 15–35 (2006)
11. Guo, Z.Y., Peng, X.Q., Moran, B.: Mechanical response of neo-Hookean fiber reinforced incompressible nonlinearly elastic solids. Int. J. Solids Struct. (2006). doi:10.1016/j.ijsolstr.2006.08.018
12. Kassianidis, F., Ogden, R.W., Merodio, J., Pence, T.J.: Azimuthal shear of a transversely isotropic elastic solid. Math. Mech. Solids **13**, 690–724 (2008)
13. Knowles, J.K., Sternberg, E.: On the ellipticity of the equations of elastostatics for a special material. J. Elast. **5**, 341–361 (1975)
14. Knowles, J.K.: On the dissipation associated with equilibrium shocks in finite elasticity. J. Elast. **9**, 131–158 (1979)
15. Knowles, J.K.: Hysteresis in stress-cycling of bars undergoing solid-solid phase transitions. Q. J. Mech. Appl. Math. **55**, 69–91 (2002)
16. Kumar, B., Chaudury, S.R.: Finite inhomogeneous shearing deformations of a transversely isotropic incompressible material. J. Elast. **51**, 81–87 (1998)
17. Merodio, J., Pence, T.J.: Kink surfaces in a directionally reinforced neo-Hookean material under plane deformation: I Mechanical equilibrium. J. Elast. **62**, 119–144 (2001)
18. Merodio, J., Pence, T.J.: Kink surfaces in a directionally reinforced neo-Hookean material under plane deformation: II Kink band stability and maximally dissipative band broadening. J. Elast. **62**, 145–170 (2001)
19. Merodio, J., Ogden, R.W.: Material instabilities in fiber-reinforced nonlinearly elastic solids under plane deformation. Arch. Mech. **54**, 525–552 (2002)
20. Merodio, J., Ogden, R.W.: Mechanical response of fiber-reinforced incompressible non-linearly elastic solids. Int. J. Non Linear Mech. **40**, 213–227 (2005)
21. Merodio, J., Saccomandi, G., Sgura, I.: The rectilinear shear of fiber-reinforced incompressible non-linearly elastic solids. I. J. Non Linear Mech. **42**, 342–354 (2007)
22. Polignone, D.A., Horgan, C.O.: Cavitation for incompressible anisotropic nonlinearly elastic spheres. J. Elast. **33**, 27–65 (1993)
23. Qiu, G.Y., Pence, T.J.: Remarks on the behavior of simple directionally reinforced incompressible nonlinearly elastic solids. J. Elast. **49**, 1–30 (1997)
24. Qiu, G.Y., Pence, T.J.: Loss of ellipticity in plane deformation of a simple directionally reinforced incompressible nonlinearly elastic solid. J. Elast. **49**, 31–63 (1997)
25. Spencer, A.J.M.: Deformations of fiber-reinforced materials. Oxford University Press, London (1972)

26. Triantafyllidis, N., Abeyaratne, R.: Instability of a finitely deformed fiber reinforced elastic material. J. Appl. Mech. **50**, 149–156 (1983)
27. Truskinovsky, L.: Structure of an isothermal discontinuity. Sov. Phys. Doklady **30**, 945–948 (1985)
28. Wineman, A.S., Pipken, A.C.: Material symmetry restrictions on constitutive equations. Arch. Rat. Mech. Anal. **17**, 184–215 (1965)
29. Zhang, J.P., Rajagopal, K.R.: Some inhomogeneous motions and deformations within the context of a non linear elastic solid. Int. J. Eng. Sci. **30**, 919–938 (1992)
30. Zee, L., Sternberg, E.: Ordinary and strong ellipticity in the equilibrium theory of incompressible hyperelastic solids. Arch. Rat. Mech. Anal. **83**, 53–90 (1983)

Seungik Baek and Thomas J. Pence
Department of Mechanical Engineering
Michigan State University
East Lansing
MI 48824-1226
USA
e-mail: pence@egr.msu.edu

Seungik Baek
e-mail: sbaek@egr.msu.edu

(Received: 19 March 2009)